Confocal Microscopy for Visualization of Skin Penetration

15

Mukul A. Ashtikar, Daya D. Verma, and Alfred Fahr

Contents

M.A. Ashtikar
Lehrstuhl für Pharmazeutische Technologie, Friedrich-Schiller-Universität Jena, Jena, Germany
e-mail: Mukul-arun.ashtikar@uni-jena.de

D.D. Verma
Novartis Pharmaceutical Corp., East Hanover, NJ, USA
e-mail: ddverma@yahoo.com

A. Fahr (✉)
Friedrich-Schiller-Universität Jena, Institut für Pharmazie, Lehrstuhl für Pharmazeutische Technologie, Lessingstraße 8, 07743 Jena, Germany
e-mail: alfred.fahr@uni-jena.de

15.1 Introduction

Over the years, various methods such as diffusion experiments (Addicks et al. 1987; du Plessis et al. 1994), microdialysis (Benfeldt 1999; Fang et al. 1999; Murakami et al. 1998; Schnetz and Fartasch 2001), visualization by microscopic techniques like conventional fluorescence microscopy (Kriwet and Müller-Goymann 1995; Yarosh et al. 1994), electron microscopy (Bouwstra and Honeywell-Nguyen 2002; Hashimoto et al. 1991; Hofland et al. 1995; Kanerva 1990; Schreiner et al. 2000; van den Bergh et al. 1999), confocal laser scanning microscopy (Betz et al. 2001; Kirjavainen et al. 1996; Schatzlein and Cevc 1998; van Kuijk-Meuwissen et al. 1998a, b; Vardaxis et al. 1997; Veiro and Cummins 1994), etc., have been exploited by researchers for studying percutaneous penetration and to gain a better understanding of the skin barrier. Tape stripping and microdialysis experiments, though extensively used to measure the amount and rate of penetration of the model compound, are lacking in providing information about the effect of the model drug on cells and lipid organization or particular pathways for the penetration of the model drug. These techniques also do not give much information about spatial distribution of the model drug inside the tissue or comment on the mechanism of penetration and more importantly, these are destructive methods where tissue has to be carefully removed or homogenized to quantify the amount of drug.

N. Dragicevic, H.I. Maibach (eds.), *Percutaneous Penetration Enhancers Drug Penetration Into/Through the Skin*, DOI 10.1007/978-3-662-53270-6_15

Electron microscopy has been extremely useful in understanding the structure of the stratum corneum (SC) and intercellular lipid organization. Bouwstra and coworkers have made important contributions to the understanding of the interactions between vesicles and human skin (Hofland et al. 1994, 1995; Schreiner et al. 2000). They employed freeze fracture electron microscopy and small angle X-ray scattering to study the effects of vesicular formulations on the SC. Their results indicated increased diffusion of the drug due to adsorption and fusion of drug-loaded vesicles to the surface of the skin. They also reported perturbations in the ultrastructure of the SC intercellular lipid domains due to mixing of liposomal components with SC lipids, which could have also enhanced penetration of the model drug. Although freeze fracture electron microscopy provides rather useful information about the effect of liposomal vesicles on the ultrastructure of the skin barrier, it lacks in providing information of penetration pathways and depth up to which the model drug has penetrated.

Another widely appreciated technique is the conventional fluorescence microscopy. Evaluation of skin treated with fluorescently labeled liposomes by fluorescence microscopy has demonstrated that the fluorescent marker remained in the SC (Kriwet and Müller-Goymann 1995) or penetrated deeper in the epidermis mainly along the hair shaft (Yarosh et al. 1994). However, during the sample preparation the tissue needs to be (cryo-) fixed which might lead to the alteration of the original specimen by the change in skin lipid organization, redistribution of the marker, etc.

Confocal microscopy has evolved over the last five to six decades and today it is an essential tool for a life-sciences laboratory; it has emerged as a sophisticated tool for tracking and studying transport phenomena of different compounds with a high degree of precision. Confocal microscopy offers significant advantages over other microscopic techniques in evaluation of thick specimens due to their inherent ability to distinguish photons generated from different focal planes of the specimen. This ability is mainly achieved in two ways, either by introducing a pinhole aperture in front of the detector which limits the out of focus light or by utilizing a nonlinear technique such as 2-photon fluorescence, which excites the specimen only in a very small focal plane at a time. Confocal microscopes create quite sharp images compared to conventional microscopes where light coming from different planes of the specimen is not differentiated, resulting in blurry and low resolution images. Confocal microscopy on a broad basis can be classified as an imaging and spectroscopic technique. Confocal techniques that are discussed in this chapter are confocal laser scanning microscopy (CLSM), two-photon microscopy, and Raman microspectroscopic techniques. Although these techniques are based on different principles, they all have something in common and that is confocality, ability to image one small focal volume at a time to construct a high-resolution image. Thanks to the modern electronics and optics, we are able to image deeper into a thick biological specimen like skin at high resolution, high speed, and in-vitro as well as in-vivo conditions. Sophisticated lasers and detection systems have enabled us to exploit nonlinear excitation phenomena such as 2-photon fluorescence, coherent anti-stokes Raman scattering, stimulated Raman scattering, etc. The following chapter reviews these techniques and discusses some of the results obtained pertaining to dermal delivery.

15.2 Confocal Laser Scanning Microscope

In the last two decades, CLSM has been extensively used as a tool to visualize the fluorescent model compounds in the skin. CLSM examination revealed valuable additional morphological information of porcine skin in wound healing studies which was not obtained by conventional microscopy (Vardaxis et al. 1997). CLSM was also used to understand the mechanism by which nanoparticulate systems facilitate skin transport. The surface images revealed that (a) polystyrene nanoparticles accumulated preferentially in the follicular openings, (b) this distribution increased

in a time-dependent manner, and (c) the follicular localization was favored by particles of smaller size (Alvarez-Roman et al. 2004). Simonetti et al. visualized diffusion pathways across the SC of native and in vitro reconstructed epidermis by using CLSM (Simonetti et al. 1995).

Many researchers used CLSM to evaluate the penetration of liposomes into human or animal skin using a fluorescent compound or a fluorescent model drug. It was demonstrated that flexible liposomes penetrated deeper into the skin in non-occlusive conditions than after occlusive application (van Kuijk-Meuwissen et al. 1998a) as measured by a fluorescent liposome marker. Touitou and coworkers examined the penetration of fluorescent probes into fibroblasts and nude mice skin by CLSM and showed that ethosomes facilitated the penetration of all probes into the cells, as evident from the high-intensity fluorescence as compared to the hydroethanolic solution or conventional liposomes (Touitou et al. 2001).

Many research groups examined different lipid combinations for their potential to influence the skin. Zellmer et al. used CLSM to demonstrate that vesicles made of native human SC lipids interact rapidly with phosphatidylserine liposomes, weakly with human SC lipid liposomes and do not interact with phosphatidylcholine (PC) liposomes (Zellmer et al. 1998). Kirjavainen et al. reported that lipophilic fluorescent marker, L-α-phosphatidylethanolamine-N-lissamine rhodamine B sulfonyl (N-Rh-PE) was able to penetrate deeper into the SC from liposomal vesicles containing dioleylphosphatidylethanolamine (DOPE) than from liposomes without DOPE. A pretreatment of the skin with unlabeled liposomes containing DOPE or lysophosphatidylcholine (lyso-PC) enhanced the subsequent penetration of the fluorescent markers, N-Rh-PE, and sulforhodamine B into the skin, suggesting a possible penetration enhancing activity (Kirjavainen et al. 1996).

Procedures like iontophoresis which enhance the percutaneous flux of model drugs like calcein (Turner and Guy 1998) and mannitol (Kirjavainen et al. 2000) were also examined by CLSM in animal models. Grams et al. used CLSM to visualize time resolved diffusion of a lipophilic dye into the hair follicle of fresh and unfixed piece of human scalp skin. The authors claimed that this technique was able to visualize the diffusion of a dye into the upper hair follicle at different time points (Grams et al. 2004). In another study, they also report that follicular accumulation of lipophilic dyes increased when applied in combination of surfactant-propylene glycol (Grams et al. 2003).

15.2.1 Principle of CLSM

Confocality is achieved in CLSM by using a point illumination and point detection. Marvin Minsky constructed the first confocal microscope in 1957 at Harvard (Semwogerere and Weeks 2008). He used a zirconium arc lamp and two pinholes, one in front of the lamp and another in front of the detector to achieve the confocality, while the sample was scanned through the light beam to generate the image. Today's confocal microscopes although different are based on the same principle of point illumination and detection, and their ability to image thick samples with high resolution have enabled their use in studying skin penetration of various molecules and delivery systems.

A CLSM can create a very sharp and high-resolution image of a specimen compared to a conventional microscope. This ability arises from the fact that CLSM is able to filter light coming from parts of the specimen that are not in focus, and in the process as much as 95 % of the light coming from the specimen can be blocked to generate an image. As a result, very few photons actually make it to the detector therefore a very high intensity light source in the form of laser is used in modern CLSMs. One disadvantage of this is that more than one laser might be required in order to have multiple excitation wavelengths.

The principle of confocality is explained in the schematic diagram in Fig. 15.1a where light coming from the specimen is focused on the detector with the help of two lenses. Due to the pinhole in front of the detector only the light coming from a very small focal point reaches the detector and light from out of focus regions of the

specimen is blocked by the pinhole. The second pinhole is employed in front of the light source, which limits the amount of specimen that is illuminated at any time, and as a result reduces the background scatter from out of focus region of the specimen. Two pinholes of the confocal microscope are able to significantly reduce the background blur and produce very high-resolution images (Hollricher and Ibach 2011; Nwaneshiudu et al. 2012).

Schematic representation of a CLSM is provided in Fig. 15.1b. In a modern CLSM, a beam of light is provided by a laser which passes through a pinhole onto a dichroic mirror which directs the light to a scanning mirror assembly and onto the specimen through the microscope objective. The scanning mirrors scan the laser across the specimen in order to generate the image. Light reflected from the specimen is de-scanned at the scanning mirrors and passes to the photo-multiplier tube (PMT) detectors through the dichroic mirror (Semwogerere and Weeks 2008). Light coming from out of focus regions of the specimen is blocked at the detector by a pinhole. The image

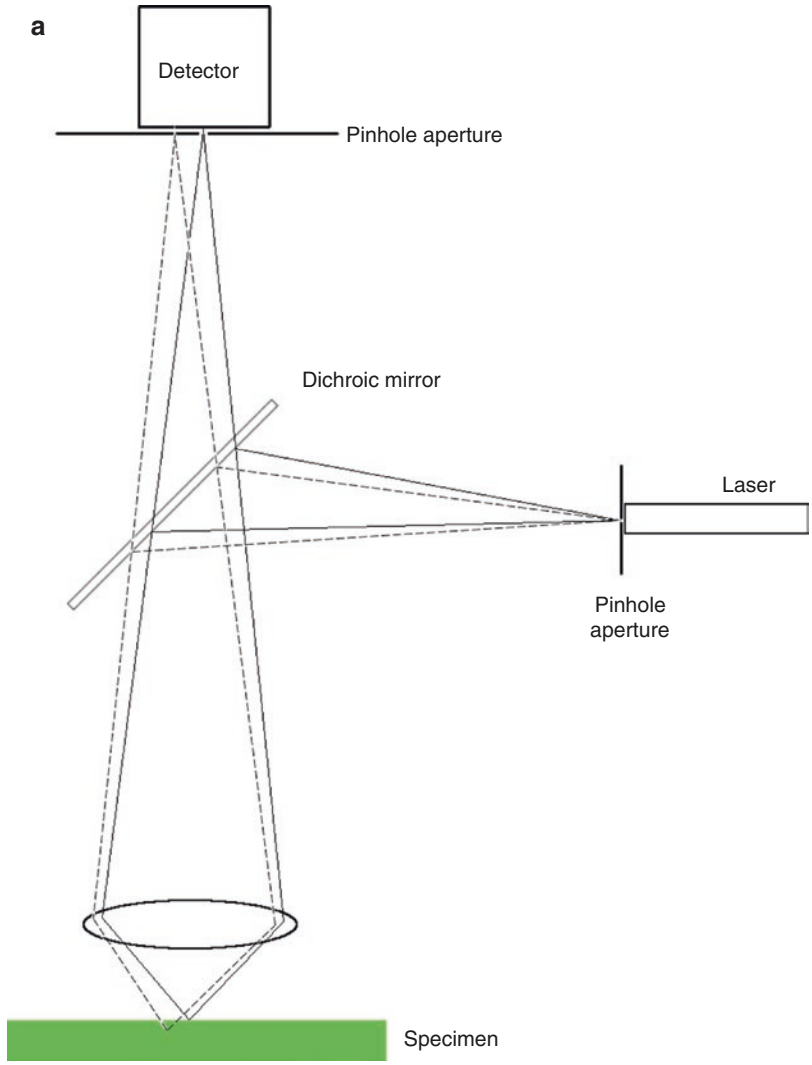

Fig. 15.1 (**a**) Pinhole in front of the detector rejects light emerging from out of focus regions. (**b**) Schematic representation of CLSM optics (Semwogerere and Weeks 2008)

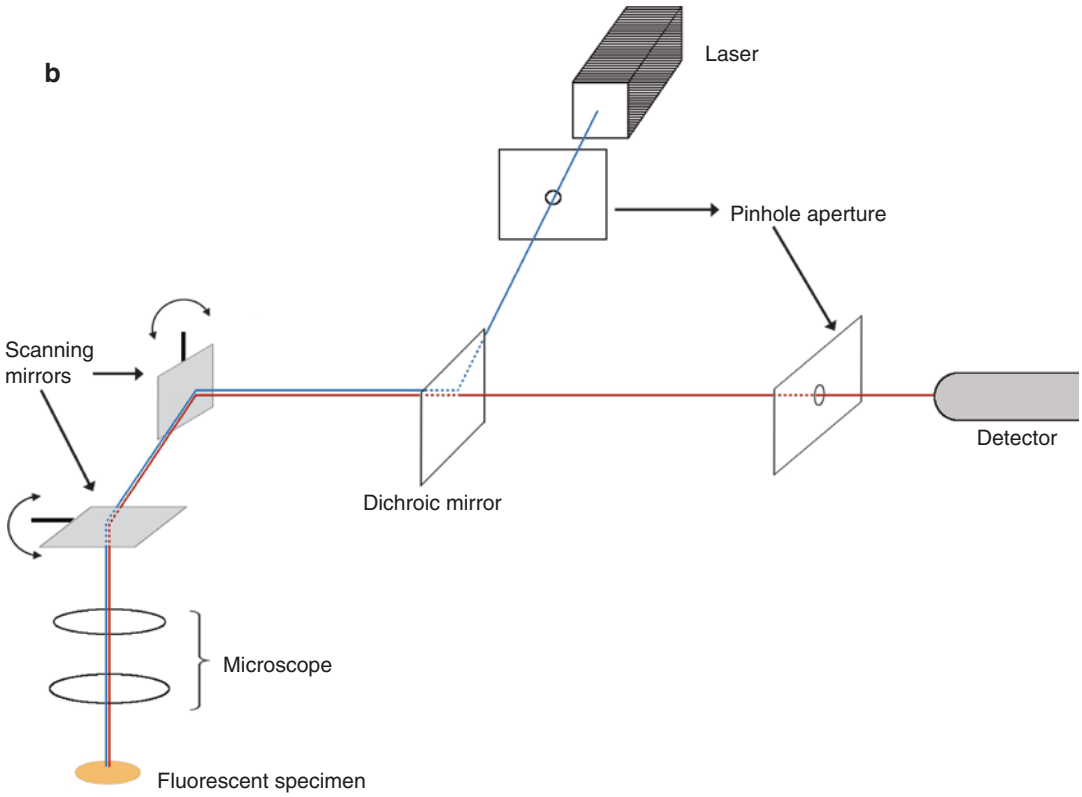

Fig. 15.1 (continued)

of the specimen is reconstructed by a computer from the spatial coordinates and corresponding light intensity at the detector.

15.2.2 Major Advantages of CLSM

Blurring effect observed in the conventional microscope is either eliminated or reduced to a great extent in CLSM, and as a result, images generated are very sharp, have a high contrast and a higher resolution. In practice a CLSM can have at best a horizontal resolution of 0.2 μm and at best a vertical resolution of 0.5 μm. Further, a 3D sectioning or optical sectioning of the sample is possible as a very small focal point is imaged at a time which also gives possibility to image thicker specimens using a confocal microscope. Using multiple lasers, it is possible to excite different fluorophores simultaneously.

15.2.3 Major Disadvantages of CLSM

CLSM has an inherent resolution limitation of about 0.2 μm and is dependent on the wavelength of excitation. Due to the high intensity light source, photo bleaching and photo-damage in the illuminated region of the specimen is possible and repeated scans with high-energy light beam greatly reduce the viability of biological tissues and thereby the available time for studying a given specimen. For a high quality image, CLSM usually needs long scan times and as a result, CLSM is not suitable for imaging rapid physiological events in a cell or a tissue. In addition, because lasers emit light only at certain narrow bandwidths, in order to be able to excite a large range of fluorophores, multiple lasers need to be employed which along with the complex electronics, scanning mirrors, and sophisticated data acquisition system raise the cost.

15.2.4 CLSM Used for Tracking Liposomal Formulations in the Skin

Liposomes have been extensively studied and suggested as a vehicle for topical drug delivery (Chen et al. 2010, 2011; Dragicevic-Curic et al. 2008, 2009; Ntimenou et al. 2012). However, the mechanism of penetration of liposomes as drug carriers into the intact skin is not fully understood. In this section, we will discuss the interactions between liposomes, containing hydrophilic and lipophilic fluorescent probes, and human as well as rat skin using CLSM.

15.2.4.1 Tracking Skin Penetration of Liposomally Entrapped or Un-entrapped Hydrophilic Fluorescent Model Drug

The mechanism of action of liposomes as penetrable drug carriers in topical delivery is not completely understood. In order to evaluate if liposomes are able to increase skin penetration of only entrapped hydrophilic drugs or also of unentrapped hydrophilic drugs, three different liposomal formulations using carboxyfluorescein (CF) as a fluorescent hydrophilic model drug were prepared: '$CF_{in\text{-}out}$' (non-entrapped CF was not removed), 'CF_{in}' (non-entrapped CF was removed), and 'CF_{out}' (a pre-calculated amount of CF was added to empty liposomes). All the liposomal formulations had a similar size of liposomes and the concentration of CF was the same in all formulations (Verma et al. 2003b). After 6 h incubation of the skin with different formulations, the skin was cryofixed and 7 μm thick sections were cut using a cryo-microtome. These cross-sections were investigated using CLSM for the skin penetration of CF.

The penetration studies and CLSM images showed that liposomes $CF_{in\text{-}out}$ exhibited maximum deposition of CF in the SC, whereas liposomes CF_{in} showed higher penetration of CF into the deeper skin layers such as the viable epidermis (Fig. 15.2), and through the skin to the acceptor compartment of the Franz diffusion cell. These results were comparable to the data obtained from tape stripping experiments. This study confirmed the assumption that liposomes $CF_{in\text{-}out}$ were not under osmotic stress and will, therefore, transfer themselves more easily into the SC. The results indicated further that phospholipid vesicles not only carry the entrapped hydrophilic substance, but also the non-encapsulated hydrophilic substance into the SC and possibly to the deeper layers of the skin. Although CLSM served as a useful tool to estimate skin penetration, CLSM images do not provide the visualization of single liposomes, so the exact mechanism of penetration of liposomes still remains an unsolved question.

15.2.4.2 Effect of Vesicle Diameter on Skin Penetration of Liposomally Entrapped Drugs

The influence of vesicle size on the penetration of fluorescently labeled liposomes into the human skin was investigated using lipophilic fluorescent label, 1,1′-dioctadecyl-3,3,3′,3′-tetramethylindocarbocyanine perchlorate (DiI) (Verma et al. 2003a). In all CLSM images (Fig. 15.3) very high fluorescence was observed in the SC, which was expected due to the lipophilic nature of the fluorescent label, DiI. This study indicated that large vesicles with a size ≥ 600 nm were not able to deliver their contents into the deeper layers of the skin. These liposomes probably stayed in/on the SC and after drying they formed a layer of lipid, which would have further strengthened the barrier properties of the SC. The liposomes with size ≤ 300 nm were able to deliver their contents to some extent into the deeper layers of the skin. However, the liposomes with size ≤ 70 nm were most promising for dermal drug delivery into the deeper skin layers as they showed maximum fluorescence both in viable epidermis, as well as in dermis.

15.2.4.3 Synergistic Penetration Enhancement Effect of Ethanol and Phospholipids on Topical Drug Delivery

It was observed that the composition of liposomal formulation had an appreciable effect on the penetration of compounds into and through the

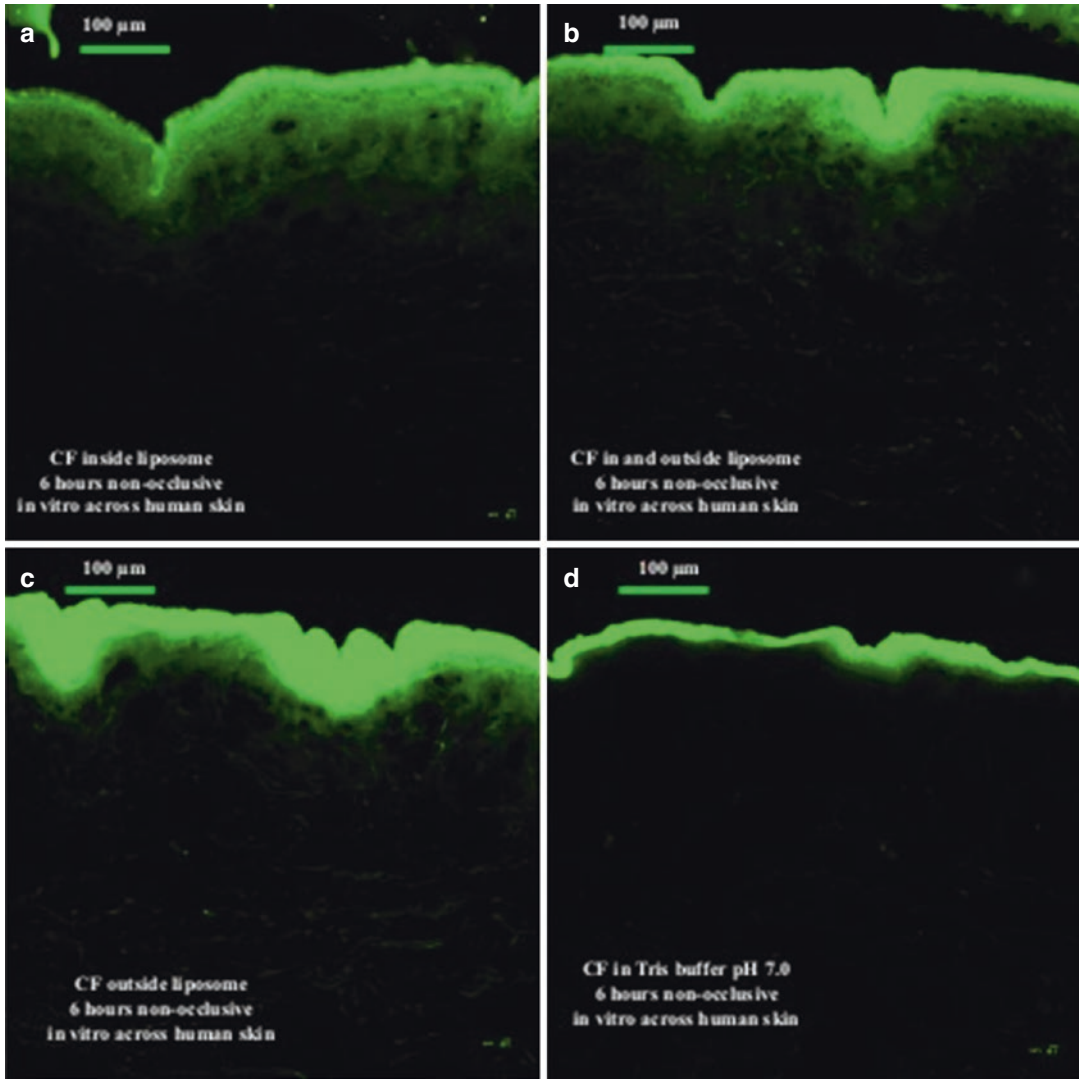

Fig. 15.2 Fluorescence micrographs of cross-sections of human abdominal skin incubated on Franz diffusion cells with different formulations containing CF. Formulations were applied without occlusion for 6 h. (**a**) Liposomes CF_{in}; (**b**) liposomes $CF_{in\text{-}out}$; (**c**) liposomes CF_{out}, CF outside liposomes; and (**d**) CF dissolved in Tris buffer. Scale bar represents 100 µm (Reprinted from Verma et al. (2003b) with permission from Elsevier)

skin (Hofland et al. 1994; Jimbo et al. 1983; Loftsson et al. 1989; Tenjarla et al. 1999). Hence, the effect of lipid vesicular systems embodying ethanol in relatively high concentrations on the percutaneous penetration of cyclosporin A (CyA) was investigated using a standardized skin stripping technique and CLSM (Verma and Fahr 2004). Ethanol has been widely reported as an efficient skin penetration enhancer in the concentration of 5–100 % (Bhatia and Singh 1999; Kobayashi et al. 1994; Simonetti et al. 1995). In a preliminary study, we have seen that not only are the amount and the type of phospholipids important for skin penetration enhancement, but also the amount of ethanol has a significant role in delivering the fluorescent model compounds into the skin (Fig. 15.4) (Verma 2002). We hypothesized that ethanol and phospholipids might have synergistic skin penetration enhancing effect.

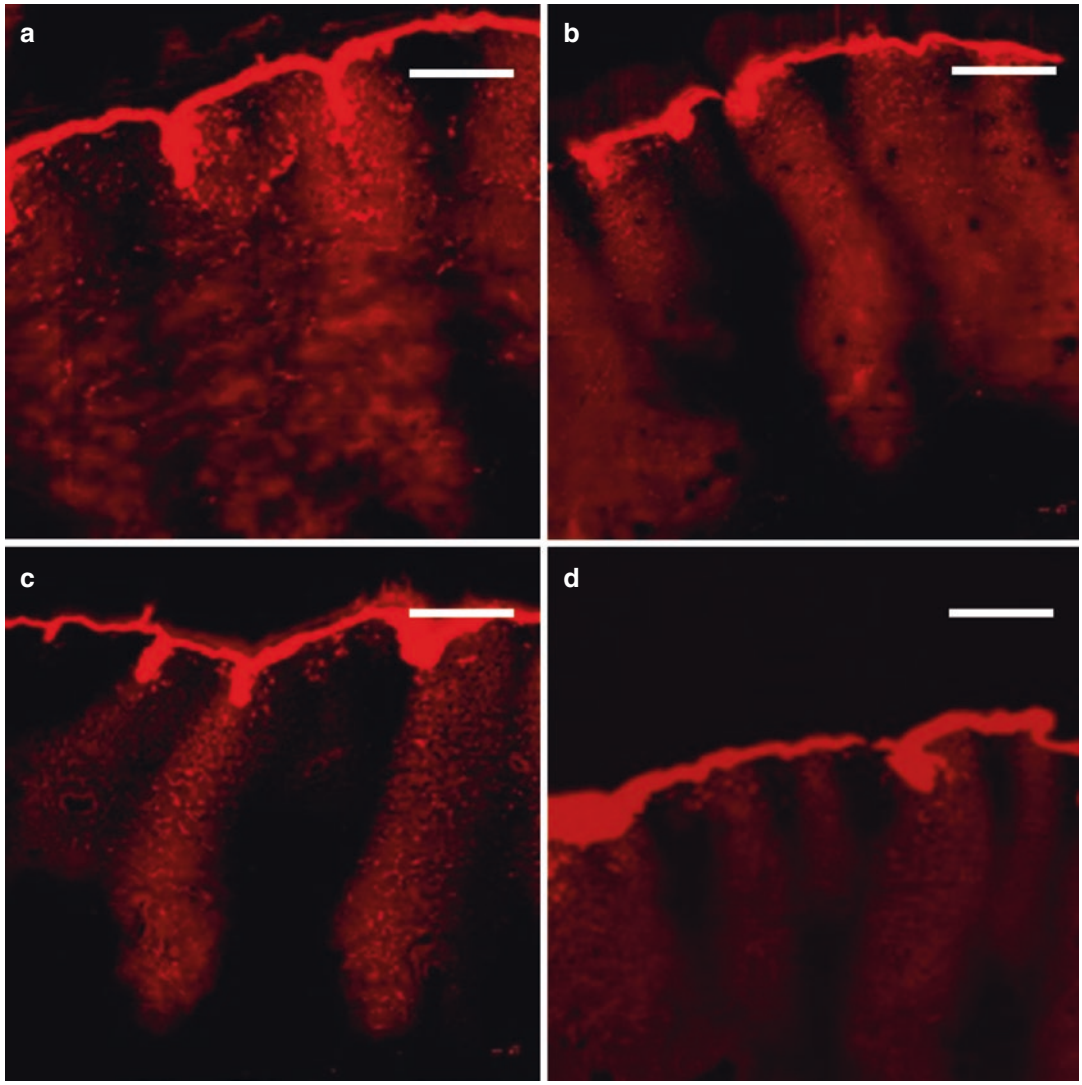

Fig. 15.3 Fluorescence micrographs of cross-sections of human abdominal skin incubated on Franz diffusion cells with different formulations containing DiI. The vesicles were applied non-occlusively for 12 h. (**a**) Ethanolic solution of DiI; (**b**) NAT8539/ethanol (10/3.3); (**c**) NAT8539/ethanol (10/10); (**d**) NAT8539/ethanol (10/20). Scale bar represents 50 μm (Reprinted from Verma et al. (2003a) with permission from Elsevier)

In order to evaluate synergistic effect of the ethanol and phospholipids on penetration of DiI, vesicles with composition of 10% (w/v) phospholipid mixture NAT 8539 (Lipoid, Germany) and ethanol at different concentrations ranging from 0 to 20% w/v were prepared. The results of the CLSM studies are represented in Fig. 15.5. Ethanolic solution of the DiI dye was able to deliver only weak fluorescence into the SC, and no fluorescence was noticeable in the viable epidermis and dermis (Fig. 15.5a). Formulation, NAT 8539/ethanol (10/3.3), produced a homogeneous bright fluorescence throughout the SC, but no fluorescence was observed in the viable epidermis and dermis (Fig. 15.5b). Formulation, NAT 8539/ethanol (10/10), produced a bright fluorescence throughout the SC with very weak to weak fluorescence observed in the viable

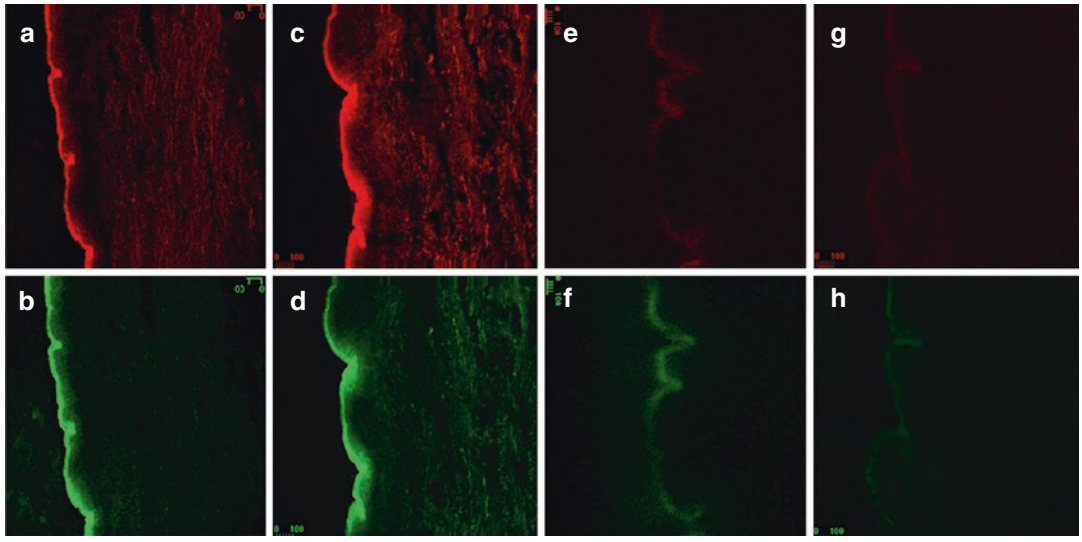

Fig. 15.4 Fluorescence micrographs of cross-sections of human skin incubated with vesicles with different lipid content for 12 h. (**a**, **b**) Ethanolic solution of N-Rh-PE (**a**) and CF (**b**). (**c**, **d**) Flexible liposomes with N-Rh-PE (**c**) and CF (**d**). (**e**, **f**) PL 90H-liposomes with N-Rh-PE (**e**) and CF (**f**); (**g**, **h**) PL25 liposomes with N-Rh-PE (**g**) and CF (**h**)

epidermis and dermis (Fig. 15.5c). Formulation NAT 8539/ethanol (10/20) produced a homogeneous bright fluorescence throughout the SC and very a weak fluorescence was noticeable in the viable epidermis and dermis (Fig. 15.5d). CLSM experiments have shown that the ethanolic solution of DiI was not even able to deliver the fluorescent label into the SC. In contrast, all the formulations with NAT 8539 and ethanol produced a bright fluorescence homogeneously throughout the SC. Formulations prepared with NAT 8539 containing 10 and 20% ethanol were also able to show very weak fluorescence in the viable epidermis and dermis. The results above were confirmed by in vitro penetration studies followed by tape stripping and extraction of the radioactively labeled CyA from various layers of the skin. Ethanol, together with NAT 8539 had synergistic effects on the delivery of the CyA into the skin, and the enhancement effect of ethanol was concentration dependent. Although CLSM images do not provide pure quantitative data regarding the skin penetration, they are, however, extremely useful as a comparative tool and give useful information about the distribution of the drug within the skin.

15.2.4.4 Terpenes as Penetration Enhancers in Liposomes

In this study, CLSM was used to investigate if incorporation of penetration enhancers (terpenes) into liposomal formulations had an effect on their percutaneous penetration enhancing ability in human and rat skin (Verma 2002). Fluorescent derivative of CyA, D-Ala-8-CS-beta-aminebenzofurazan (Fl-CyA) and DiI, were used as lipophilic markers while Alexa Fluor-488® (Life Technologies GmbH, Germany) was used as a hydrophilic fluorescent marker. Vesicles with and without terpenes were compared with ethanolic and hydro-alcoholic solutions of the fluorescent labels. Double-labeled vesicles, vesicles containing both DiI and Alexa Fluor-488®, were applied to skin for 6 and 12 h. Penetration of the fluorescent labels was visualized by CLSM both in terms of depth and intensities of the fluorescence. Fluorescent intensities of the CLSM images were semi-quantitatively scored ranging from no fluorescence to bright fluorescence. Further details regarding imaging and formulations can be found elsewhere (Verma 2002).

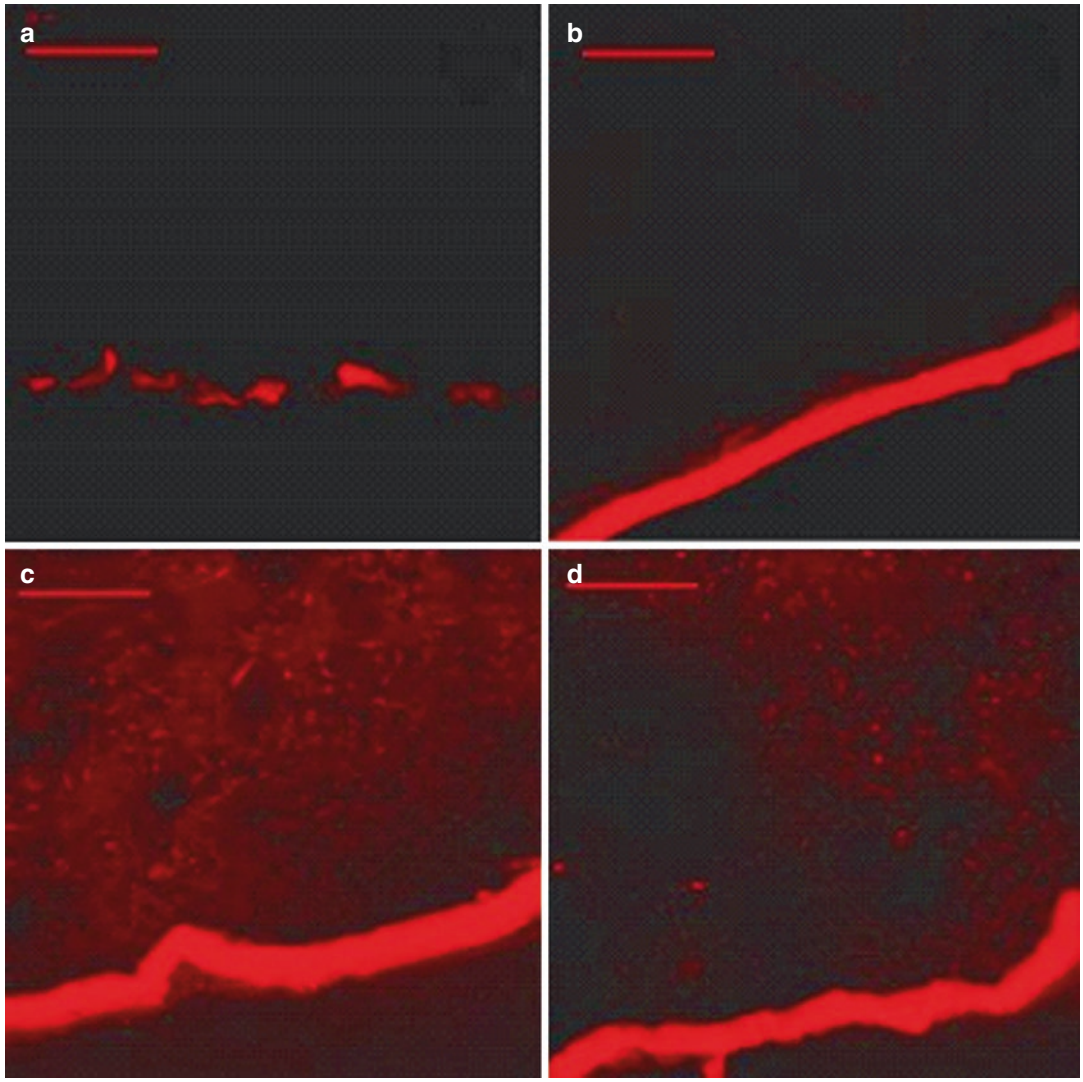

Fig. 15.5 Fluorescence micrographs of cross-sections of human abdominal skin incubated on Franz diffusion cells with different formulations containing DiI. The vesicles were applied without occlusion for 12 h. (**a**) Ethanolic solution of DiI; (**b**) NAT8539/ethanol (10/3.3); (**c**) NAT8539/ethanol (10/10); (**d**) NAT8539/ethanol (10/20). Scale bar represents 50 μm (Reprinted from Verma and Fahr (2004) with permission from Elsevier)

CLSM images of cross-sections of rat skin incubated for 6 h with Fl-CyA liposomes prepared with and without terpenes are compared in Fig. 15.6. A bright fluorescence was observed in the SC (Fig. 15.6b) for skin treated with Fl-CyA liposomes without terpenes, but only a negligible or no fluorescence was observed in the viable epidermis and dermis. The skin treated with Fl-CyA liposomes containing 1 % terpenes showed a relatively higher fluorescence in the SC and weak fluorescence in the epidermis, suggesting diffusion of the Fl-CyA from SC to the epidermis (Fig. 15.6c). Ethanolic solution of Fl-CyA showed a very weak fluorescence in the SC and no fluorescence was observed in the viable epidermis and dermis (Fig. 15.6a). Based on the fluorescence scores obtained from CLSM images, results indicate that penetration enhancers do play an important role in the penetration of fluorescent labels into the skin.

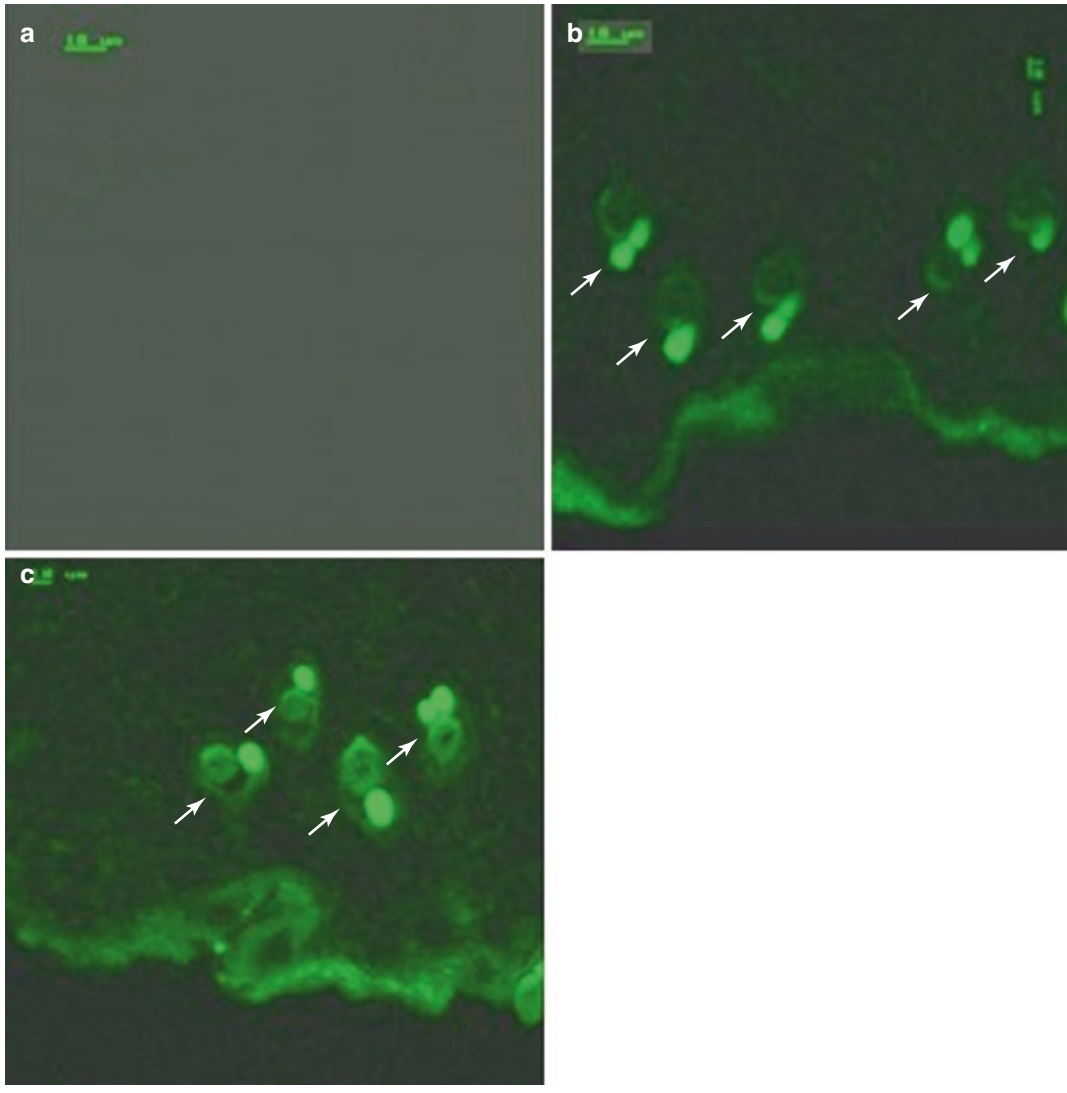

Fig. 15.6 Cross-sections of rat skin incubated with different formulations containing Fl-CyA. The vesicles were applied non-occlusively for 6 h on rat skin. (**a**) Ethanolic solution of Fl-CyA, (**b**) Fl-CyA liposomes without terpenes, and (**c**) liposomes containing 1% terpenes. The length bar represents 10 μm. *Arrows* represent hair follicles in the dermis

Cross-sections of human skin treated with double-labeled (DiI and Alexa Fluor 488®) liposomes with and without terpenes are represented in Fig. 15.7. Incubation period of formulation with the skin was 6 h (Fig. 15.7a–c) and 12 h (Fig. 15.7d–f). Control was provided by skin samples treated with hydro-alcoholic solution containing both dyes mentioned above. In all the samples, the fluorescence was restricted mainly to the SC and to a smaller or larger extent, to the viable epidermis. Samples treated with hydro-alcoholic solutions of the dyes exhibited fluorescence for both DiI and Alexa Fluor-488® only in the SC. Increasing the incubation period from 6 h to 12 h only increased the fluorescence intensities for both the labels (Fig. 15.7a, d). In samples treated with dual labeled liposomes without terpenes, fluorescent markers after 6 h diffusion are restricted to the SC only. DiI penetrated up to deeper layers of the SC however no fluorescence

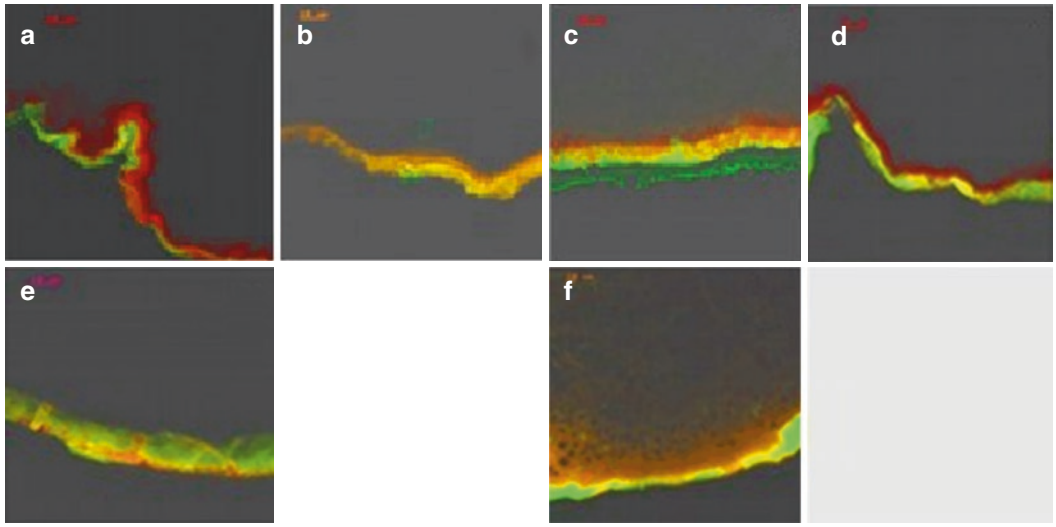

Fig. 15.7 Cross-sections of human abdominal skin treated with formulations containing two fluorescent markers, DiI and Alexa Fluor 488®. The formulations were applied without occlusion for 6 h (**a**–**c**) and 12 h (**d**–**f**). (**a**, **c**) Hydro-alcoholic solution of DiI and Alexa Fluor 488, (**b**, **e**): double-labeled liposomes without terpenes (**c**, **f**): double-labeled vesicles containing 1 % terpenes. The bar represents 10 μm

was observed in the viable epidermis and dermis (Fig. 15.7b). Increasing the incubation period to 12 h did not have marked improvement in penetration depths. CLSM images (Fig. 15.7e) show higher intensities and slightly higher penetration up to viable epidermis achieved for both the dyes. Although distribution of Alexa Fluor-488® appears uniform for both 6 and 12 h diffusion samples, distribution of lipophilic dye DiI was not uniform for 12 h samples. For skin treated with liposomal formulations containing 1 % terpenes, much higher intensities were observed for both the fluorescent dyes in the SC (Fig. 15.7c, f). For sample with 6 h incubation, very weak fluorescence for Alexa Fluor-488® while weak fluorescence for DiI was observed in the viable epidermis. For 12 h incubation samples, fluorescence intensity scores were bright-fluorescence at SC for both the dyes and moderate fluorescence intensities were observed in the viable epidermis. Surprisingly, the reddish fluorescence continued from the epidermis toward the dermis, indicating a diffusion of the lipophilic marker. It was observed that liposomal formulations containing terpenes as penetration enhancers were able to deliver relatively higher amounts of fluorescent labels into the SC, epidermis, and to a small extent the dermis. In this study, we clearly demonstrated the ability of CLSM to simultaneously image two fluorescent dyes.

15.2.5 Tracking the Penetration of Fluorescence Labels into Hair Follicles

15.2.5.1 Tracking of Fluorescently Labeled Cyclosporin A into Rat Hair Follicles

CLSM has been successfully used to track the follicular penetration of drugs. Topical application of the CF-loaded liposomes has been reported to significantly increase the accumulation of CF in the pilosebaceous units compared to other non-liposomal formulations (Lieb et al. 1992). Using CLSM, Patzelt et al. demonstrated that follicular penetration for nanoparticles was size dependent (Patzelt et al. 2011).

The effect of terpenes as penetration enhancers in liposomes for targeting hair follicles was

investigated using Fl-CyA vesicles (as mentioned above), with and without terpenes, in rat skin. Figure 15.6 also depicts the role of the pilosebaceous unit in the penetration of drugs into the skin. A bright fluorescence was observed in the pilosebaceous units (bright green fluorescent regions in dermis in Fig. 15.6b, c identified as the hair shaft, a part of the pilosebaceous unit) for both formulations, with and without PE. The fluorescence was also visualized in the outer root sheath of the hair shaft (Figs. 15.6b–c and 15.8) (Verma 2002). The images presented here demonstrate that the liposomal vesicles can enter the pilosebaceous unit and deliver their content to the hair follicle and possibly to the hair bulb. The importance of this was stressed upon by the fact that ethanolic solution of Fl-CyA failed to deliver any fluorescence into the skin. These CLSM results were supported by in vivo studies with Dundee Experimental Bald Rats model (Verma et al. 2004) and other published reports (Agarwal et al. 2000; Bohm and Luger 1998; Lieb et al. 1992; Niemiec et al. 1995). The CLSM investigations enabled us to visualize the accumulation of fluorescent label in the pilosebaceous units, which is not possible with tape stripping.

15.2.5.2 Accumulation of CF and N-Rho-PE Loaded Liposomes in the Human Hair Follicles

In this study, liposomal formulations containing CF and N-Rh-PE were prepared (Verma 2002). Liposomal formulations were able to deliver both the hydrophilic and lipophilic fluorescent labels to the human hair follicles as seen in Fig. 15.9a, b. Studies represented in Figs. 15.6, 15.8, and 15.9 demonstrated that the presence of hair follicles plays a significant role in the skin penetration of drugs, as well as that the presence of penetration enhancers helps the formulation in enhancing the follicle delivery of drugs.

15.2.6 The Efficacy of Dermaroller® to Enhance Penetration into the Skin

CLSM was also used to investigate the efficacy of the micro-perforation devices, Dermaroller® (Horst Liebl ETS, France), in increasing the skin penetration of a fluorescent lipophilic model compound DiI encapsulated in liposomes (Verma 2002). Three types of Dermarollers® were tested in this study, namely, Dermaroller® C8 0.13–15°,

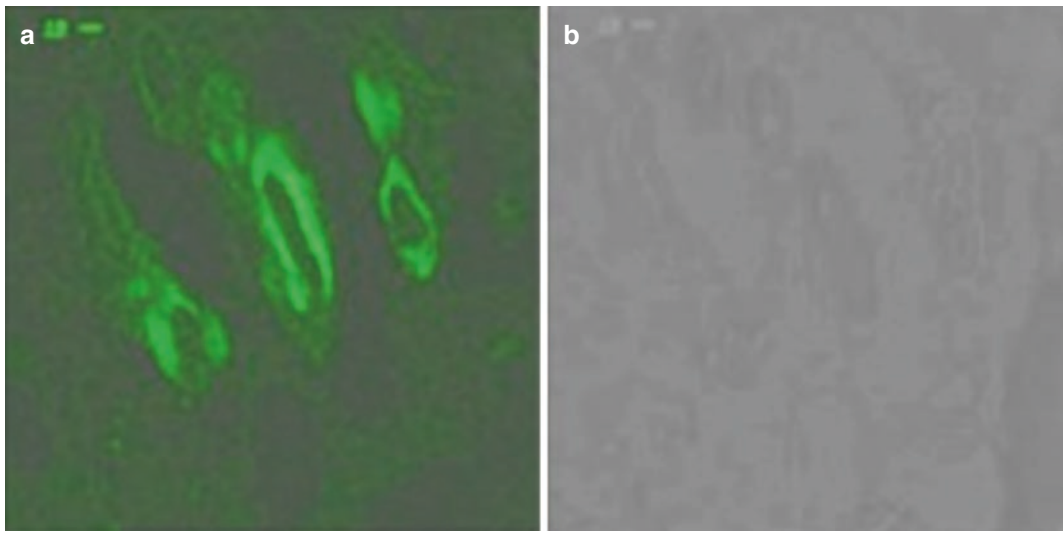

Fig. 15.8 Fl-CyA liposomes treated rat skin cross-section demonstrating the role of pilosebaceous units in the penetration of substance into the skin. The bar represents 10 μm. (**a**) Fluorescence micrograph and (**b**) transmission-mode image of the cross-section

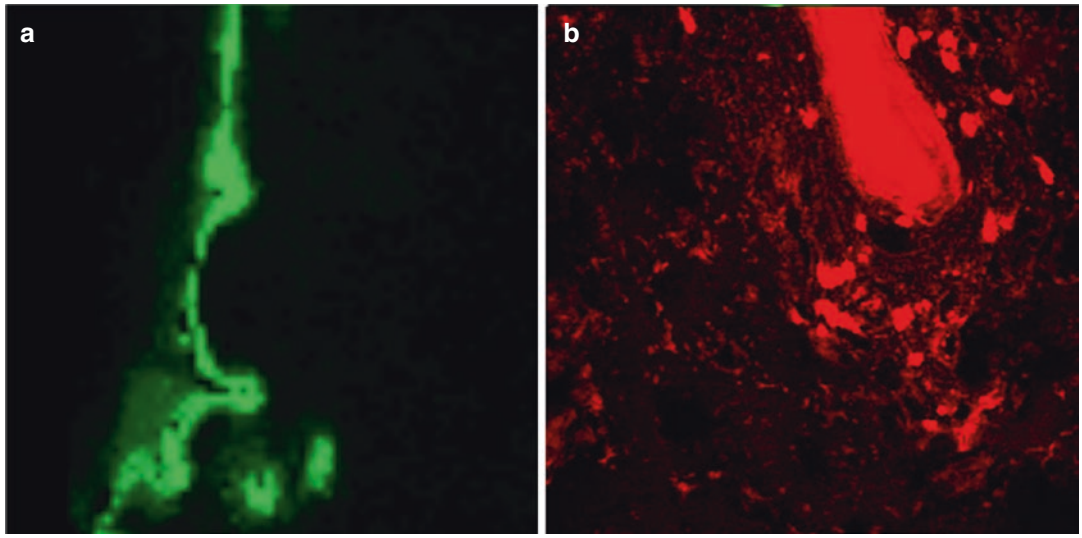

Fig. 15.9 Fluorescence micrographs showing (**a**) CF delivery to hair follicles and (**b**) high-resolution micrograph showing rhodamine delivery to hair follicle following topical application of fluorescent liposomes

M8 1.5–15°, and M8 1.5–30°. Control was provided by the skin not treated with Dermarollers®.

Bright intensity of fluorescence was observed in SC for all samples treated with Dermaroller and for control (Fig. 15.10). For control samples, however, fluorescence intensities in the viable epidermis and dermis were very low. For Dermaroller® C8 0.13–15°, highest fluorescence was observed in the SC and fluorescence intensities rapidly decreased in the viable epidermis and dermis (Fig. 15.10b). Dermaroller® C8 0.13–15° was intended for delivering drugs to the SC whereas Dermaroller® M8 1.5–15° and M8 1.5–30° were optimized for delivering drugs to the deeper regions of skin. Both M8 Dermarollers® did show very high fluorescence intensities in the dermis region (Fig. 15.10c, d). We observed that samples treated with both M8 Dermarollers® showed only a weak fluorescence in the viable epidermis region and showed weak lateral diffusion of the fluorescent label from the pores. This might be because Dermaroller® was able to deliver the liposomes into the deeper layers quickly during application of the Dermaroller but after the application, liposomes probably were not able to diffuse to a great extent from the surface of the skin to the deeper layers in the skin. In this study, we emphasized on the spatial distribution of the fluorescent label which helped us to get a better understanding of the mode of action of the micro-perforation device, Dermaroller®.

15.3 Two-Photon Fluorescence Microscopy

15.3.1 Principle of Two-Photon Fluorescence Microscopy

As seen from aforementioned studies, CLSM is a very good technique for the imaging of biological samples; however, it suffers from some disadvantages. One of the most important limitations of the CLSM is that because only a small fraction of the incident light reaches the detector, relatively high intensities of light are required to achieve high signal to noise ratios. This results in high total energy transfer to the specimen during imaging. Also, the laser beam excites the fluorophores in the specimen above and below the focal plane that is under investigation and this can cause severe photo bleaching, photo damage, and even dehydration of the biological specimen. Many fluorophores generate free radicles or singlet oxygen when excited which can be toxic if imaging living cells or tissue. CLSM also suffers from low axial resolution especially when imaging deep within a thick

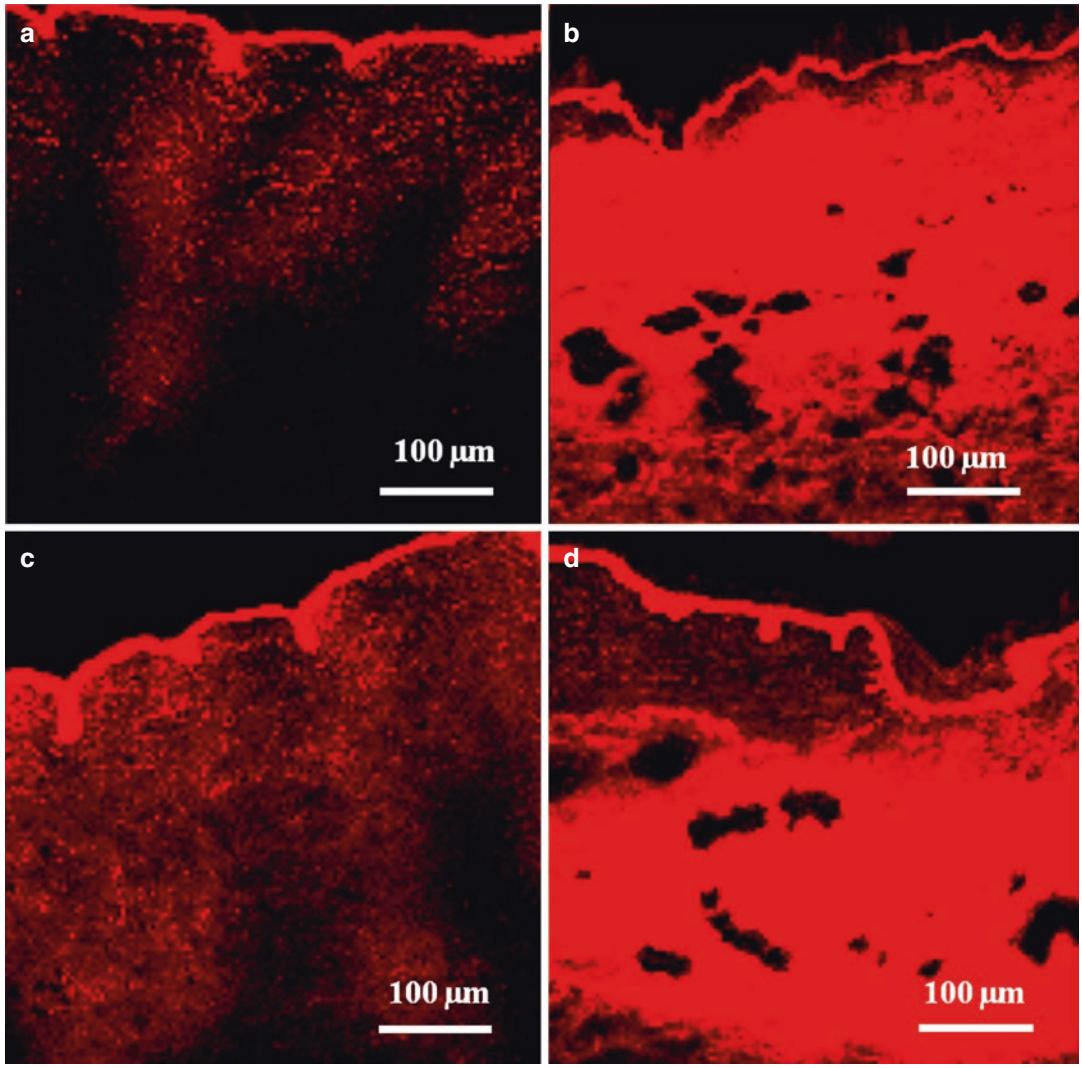

Fig. 15.10 Fluorescent micrographs of cross-sections of human abdominal skin pretreated with Dermaroller® and incubated on a Franz diffusion cell with liposomes containing lipophilic fluorescent label DiI. The liposomes were applied without occlusion for 3 h. (**a**) Control; (**b**) Model C 8 0.13–15°; (**c**) Model M 8 1.5–15°; (**d**) Model M 8 1.5–30°

tissue. The poor axial resolution results from the scattering of light by the specimen itself, which can lead to detection of light that is not generated from the observed focal plane. Also CLSM employs short wavelength excitation sources and shorter wavelengths are scattered stronger (scattering intensity is inversely proportional to fourth power of the wavelength) hence these excitation sources are not very efficient at deep tissue imaging.

Due to limitations in deep tissue imaging, when adopting a CLSM for imaging skin, the sample must be cryo-sectioned and this is not always possible and desirable.

Multiphoton excitation phenomenon was proposed in 1931; however, Kaiser and Garret were able to validate it only in 1961 after the development of lasers which were sufficiently powerful to generate the high photon flux required for two-photon excitation. Figure 15.11a explains the

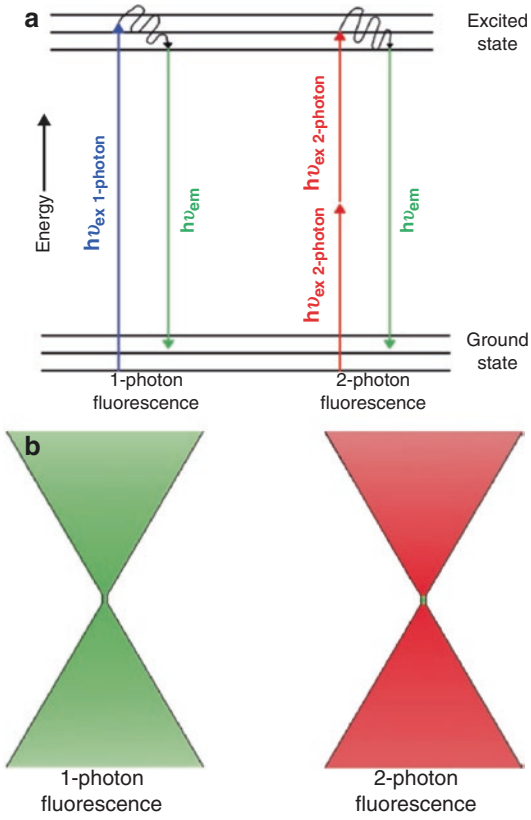

Fig. 15.11 (**a**) Jablonski diagram elucidating the differences between single photon fluorescence and two photon fluorescence phenomenon. (**b**) Excitation volume in one-photon and two-photon fluorescence phenomena

energy transfer during one-photon and two-photon excitation. In single-photon fluorescence, the fluorescence photon is generated when a high energy photon is incident on the fluorophore, which results in raising the energy level of one of the electrons to an excited state. In two-photon excitation, if two low energy photons arrive together within 10^{-18} s of one another, the combined energy transfer of the two low energy photons is sufficient to raise the same electron to a higher energy level (Dunn and Young 2006). A low energy photon is too weak to illicit the two-photon fluorescence phenomenon in the fluorophore. Hence, in order to increase the probability of simultaneous incidence of photons a laser with very high photon flux is required. Setup of a two-photon microscope is quite similar to that of a confocal scanning microscope with two major differences. One is the light source, two-photon microscopes use a tunable Ti-sapphire high frequency pulsed laser which has a pulse length of approximately a few hundred femtoseconds. The second important difference is the lack of any pinholes in front of the detector to avoid detecting scattered light from out of focus plane.

One of the important advantages of 2-PFM is that total energy delivered to the specimen is much lower as compared to a CLSM. Also the two-photon excitation phenomenon occurs only at a very small focal volume (Fig. 15.11b) and as a result fluorophores in a very small volume of the specimen are excited, which reduces the probability of photo-bleaching, photo-damage. In addition, no confocal pinhole aperture is required to block the scattered light from out of focus planes. The near-infrared (NIR) light source used in a 2-PFM is very efficient at imaging deeper regions of the biological samples, as it is least scattered and absorbed by the biological samples. These advantages mean that the skin samples can be studied without cryofixing and cutting.

Disadvantages of a two-photon microscope include a relatively high price of the ultra-short pulsed Ti-sapphire lasers and the fact that they require an elaborate cooling system. Also, 2-PFM has lower lateral resolution compared to CLSM, but in practice the difference in their resolution is not significant.

15.3.2 Application of Two-Photon Microscopy in Skin Penetration Experiments

Carrer et al. used 2-PFM to study the architecture and physical properties of the pig skin epidermis and permeability of different liposomal formulations in the pig skin (Carrer et al. 2008). In this study, authors were able to easily distinguish different layers of the pig epidermis based on their morphological differences without any significant sample preparation. To study the hydration/polarity of different layers of the

epidermis they used Laurdan generalized polarization (Laurdan-GP) values as an indicator of polarity. As expected, the Laurdan-GP values were highest for SC and decreased for deeper layers of the skin indicating an increase in fluidity or hydration. The authors report an interesting observation in the intercluster region (canyons or wrinkles as in human skin), the Laurdan-GP values in the canyons were quiet high, comparable to that of SC, and they did not change with depth (from surface of SC to dermis), indicating that canyons might show environment similar to SC. To study the penetration of liposomal formulations, Lissamine rhodamine B 1,2-dihexad ecanoyl-*sn*-glycero-3-phosphoethanolamine was incorporated in the liposomal membrane. After 16-h diffusion, image stacks were collected and penetration was measured in the form of ratio of fluorescence intensity of rhodamine and autofluorescence of the skin. Authors report that the liposomes with lower lipid content (10 mg/ml) were able to deliver more fluorescent label to the lower parts of viable epidermis compared to the formulations with higher lipid content (25 and 50 mg/ml).

van den Bergh et al. elucidated the mechanism of interactions of elastic and rigid liposomal vesicles with human skin (van den Bergh et al. 1999). Using 2-PFM and different electron microscopic techniques they studied interactions between skin and various elastic liposomal formulations to understand the modulation of the skin barrier. They observed that fluorescently labeled elastic vesicles primarily affected the intercellular lipid lamellae of the SC, while the underlying layers of the viable epidermis remained relatively unchanged. This effect was visualized using 2-PFM, in the form of small penetration pathways that were confined to the SC only. Authors also reported that the penetration enhancing ability of elastic vesicles was dependent on whether vesicles were applied with or without occlusion.

Oleic acid is a good penetration enhancer and has been found to increase transdermal penetration of both hydrophilic and hydrophobic drugs by modulating the intercellular lipid domains in the SC. Yu et al. used a high-speed two-photon microscope with dual channels capable of simultaneous monitoring of autofluorescence of skin and fluorescence from rhodamine as a model drug (Yu et al. 2003). Treatment of human skin with oleic acid as a penetration enhancer was found to induce increased intra-corneocyte diffusion of the hydrophilic model drug (sulforhodamine-B), while causing localization of the hydrophobic model drug (Rhodamine-B hexyl ester) to the intercellular region. Hence, Yu et al. provided evidence that for chemical penetration enhancers, intra-corneocyte diffusion is an important enhancement mechanism along with fluidization of intercellular lipid domains, and physicochemical properties of the drug would determine which pathway predominates in the penetration enhancement.

In 2002, Jenlab GmbH introduced a dual-channeled noninvasive multi-photon tomograph capable of in vivo optical biopsies with subcellular spatial resolution based on near-IR femtosecond pulsed laser. König et al. reported the potential of this microscope to acquire high-resolution images from deep within the skin in vitro and in vivo (Konig et al. 2006; Schenke-Layland et al. 2006). The microscope utilized the second harmonic generation (SHG) signal to monitor the position of the microscope in the skin, while the fluorescence channel was used to detect either autofluorescence from the NAD(P)H, flavins, melanin, etc., or to detect exogenous fluorophores. In vivo imaging capabilities of 2-PFM promises great advances in cancer diagnostics and skin diseases, as well as in understanding the mechanisms involved in dermal drug delivery.

2-PFM is, as already mentioned, a relatively young technology. Bio-Rad Laboratories (USA) introduced the first commercial two-photon microscope in 1996 and since then this technology has seen exponential growth in its use and applications. Its ability to take high-resolution optical biopsies of the intact skin or even do live imaging in vivo holds a great potential to unlock the secrets that were kept in the dark by nature.

15.4 Confocal Raman Microscopy

15.4.1 Principles of Raman Microscopy

Fluorescence microscopy has seen a lot of evolution in the last couple of decades and modern microscopic techniques, like CLSM, multiphoton microscopy, and various imaging modes such as fluorescence life-time imaging, Förster resonance energy transfer, etc., have increased the applications and flexibility of the fluorescence imaging. However, fluorescence microscopy still has certain disadvantages; mainly, fluorescence microscopy still utilizes exogenous dyes to label the drug or formulation. These labels are often toxic or could cause perturbations in the cells or other physiological processes. The biggest limitation for studying skin penetration is that often the fluorescent label and the formulation or the drug do not travel together and consequently fluorescence imaging could give incorrect interpretation of the observations.

Due to the disadvantages of fluorescent labeling to monitor the penetration depth in the skin, label-free vibrational spectroscopic techniques have gained importance. Vibrational spectroscopy is an identification technique based on the principle that it is possible to interfere with the vibrational state of a molecule by irradiating it with light of certain frequencies. Such interactions can be recorded in the form of spectra which are representative of the bonds present in the molecule. Because each molecule has its unique atomic structure and as a result a characteristic vibrational state, the vibrational spectra can provide a host of information about the structure of the molecule. Vibrational spectroscopy involves different techniques such as mid infrared (IR) spectroscopy, NIR spectroscopy, Raman spectroscopy, etc., but for this chapter we shall only review the Raman spectroscopic techniques. In addition, because water content in the biological specimen interferes strongly with IR spectroscopy, Raman techniques are more suitable for studying the drug penetration into the skin.

When a monochromatic beam of light is incident on the sample, most of the light is scattered by the sample such that the scattered light has the same wavelength as the incident light; this phenomenon is known as elastic scattering or Rayleigh scattering. However, a small fraction of photons do interact with the molecules of the sample and as a result, scattered photons have a different energy compared to the incident photons which manifests in the form of a shift in the wavelength of the scattered photons. This phenomenon is known as inelastic scattering or Raman scattering. Raman effect was first observed by C.V. Raman in 1928 (Raman and Krishnan 1928). It is a very weak phenomenon, about one photon undergoes Raman scattering in a million Rayleigh scattered photons. Due to low signal to noise ratio, Raman spectroscopic techniques were not very practical as they needed an intense source of light and a sophisticated detection system. After the discovery of lasers and charged coupled detectors (CCD), however, Raman spectroscopy has seen tremendous increase in its application (Hollricher 2011).

To understand the Raman effect, we shall first have a look at the Rayleigh scatter. According to the classical theory, when photons are incident on the sample, they are absorbed by the molecules of the sample and are excited to a virtual state. When molecules relax back, if they relax to the same energy level as they started in, the emitted photons have the same energy as the incident photons and this type of scattering is called Rayleigh scattering. This effect is explained schematically in Fig. 15.12. In Raman scattering, a molecule relaxes back to a higher energy level after absorbing a photon, and as a result the emitted photon has lower energy by an amount required to vibrationally excite the molecule. Reemitted photon exhibits red shift and hence this effect is also called ‘Stokes Raman scattering’. If after absorbing the photon the molecule loses a fraction of vibrational energy, i.e., if the molecule relaxes back to a lower energy state compared to its energy state before absorbing the photon, then the emitted photon has higher energy compared to the incident photon. This phenomenon is called the ‘anti-stokes Raman scattering’. Raman spectrum is a plot of

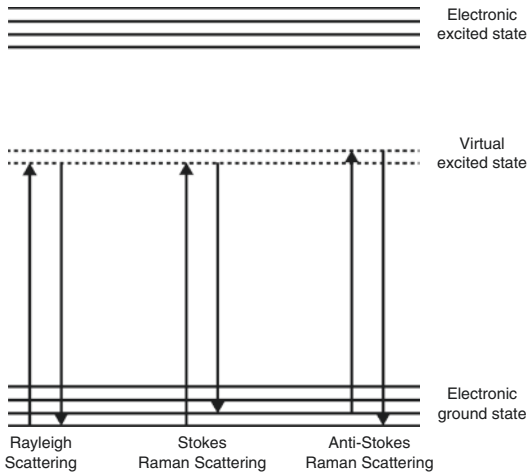

Fig. 15.12 Jablonski diagram representation of Rayleigh and Raman scattering

wavenumber shifts observed between Raman radiation and excitation radiation. Raman effect and fluorescence are distinct phenomena, in the latter, incident photons are absorbed and molecules transition from ground state to an electronic excited state due to the resonance between the vibrational frequency of the molecule and incident photons. As a result for a given molecule, fluorescence can be observed only at a certain fixed frequency range. However, Raman effect is not a resonant effect and can take place for a wider range of excitation wavelengths. In addition, fluorescence phenomenon lasts much longer in terms of few nanoseconds, while Raman scattering is much short lived, i.e., less than a picosecond.

In modern Raman microscopes, the light source is provided by a laser and is focused onto the sample with the help of an objective with high numerical aperture. Scattered light is collected by the same objective and passed through a dichroic mirror then to a spectrometer to resolve the Raman shifts, which are detected by a sensitive CCD camera. The Raman map of the sample is usually generated by scanning the sample with the help of a piezo driven stage through the laser beam. In order to improve the signal to noise ratio, most microscopes employ a confocal detection to reduce the scattered light from out of focus planes. Raman scattering intensity is proportional to the fourth power of the frequency of incident photons. Hence, excitation at 400 nm would give a 16 times more intense Raman signal compared to excitation at 800 nm (Hollricher 2011). However, skin has a very strong autofluorescence in the range of 400–700 nm and hence lower wavelengths are not ideal for Raman mapping of the skin. Although Longer wavelengths are useful for imaging thick specimen, in a diffraction-limited system they are also associated with lower spatial resolution. As a result, selecting the right wavelength of excitation is very important in order to maintain a good balance between resolution and signal quality. For collecting Raman spectra from skin, usually lasers with wavelength of 633, 660, or 785 nm are preferred.

15.4.2 Confocal Raman Microscopy for Skin Penetration Experiments

There are several studies which report application of confocal Raman microscopy (CRM) in determining the penetration of various ingredients into the skin, such as retinol (Failloux et al. 2004; Forster et al. 2011; Mélot et al. 2009), dimethyl sulfoxide (Caspers et al. 2002), water (Caspers et al. 2000), urea (Wascotte et al. 2007), 5-fluorouracil (Zhang et al. 2007), etc. Xiao et al. demonstrated the ability of CRM to study and understand the penetration mechanism of phospholipids from liposomal formulations, in pig skin (Xiao et al. 2005). Penetration of two liposomal formulations was tested, liposomes in gel crystalline state were prepared from 1,2-dipalmitoyl (d62)-sn-glycero-3-phosphocholine (DPPC-d62), while liposomes in liquid crystalline state were prepared from 1-palmitoyl(d31)-2-oleoyl-sn-glycero-3-phosphocholine (P-d_{31}OPC). After the application of liposomes to pig skin, Raman spectra were obtained using a CRM employing laser at 785 nm and spectra were recorded in the region of 100 – 3450 cm^{-1}. Exogenous phospholipids were monitored by observing the CD_2 and CD_3 stretching vibration bands at 2080 and 2220 cm^{-1}, respectively, while the skin was moni-

tored using the Phenylalanine-ring breathing mode at 1004 cm^{-1} and the amide-I band at 1652 cm^{-1}. The results indicated that the liquid state phospholipid P-d_{31}OPC penetrated 40–48 μm deep into the skin as compared to the gel state phospholipid DPPC-$d_{62,}$ which was found to penetrate only 10–15 μm deep.

We reported a method for recording depth profiles using CRM in excised human skin biopsies to study diffusion patterns of drugs and components of the formulation system (Ashtikar et al. 2012). Figure 15.13 shows a XZ-penetration profile, where every pixel represents intensity of Raman signal obtained from intact human skin treated with deuterated invasomes (P-d_{31}OPC). The depth profile scans (XZ-scans) were collected using WITec Alpha 300R CRM. Excitation was provided by 785 nm laser and step size for collecting the depth profiles was 1 μm with illumination time of 0.5s/spectra. In Fig. 15.13b, the penetration profile of deuterated phospholipid is plotted as a gradient from red to yellow, where the red color corresponds to the highest concentration of P-d_{31}OPC. The protein distribution of the skin is plotted in blue. Spectra corresponding to the invasomes and stratum corneum are represented in Fig. 15.13c. The penetration profile was constructed using spectral un-mixing algorithm, vertex component analysis, which decomposes a given dataset into fractions of most dissimilar spectral information and reconstructs the image by plotting their individual abundances (Du et al. 2008; Winter 1999). P-d_{31}OPC penetrated to a depth of ~10–15 μm after application of flexible invasomes; also it was interesting to note that the penetration profile of the phospholipid was not uniform throughout the stratum corneum.

Retinol is a common ingredient of the anti-aging creams, which is highly lipophilic and does not penetrate the skin very well. Raman microscopy is widely employed for studying penetration profiles of retinol as it has a characteristic Raman peak at 1594 cm^{-1}, which can easily be traced through the various layers of the skin. In vitro penetration profile of retinol in human skin biopsies was studied by Failloux et al. using CRM. They have reported that retinol penetrated the SC faster when it was applied in the form of microspheres as compared to an oil in water emulsion (Failloux et al. 2004). Förster et al. studied the penetration of retinol from various emulsions and also monitored penetration of oil and aqueous components of the emulsion by using D(26)-n-dodecane and deuterated water, respectively. Their results show that retinol penetration from an emulsion depends on the nature

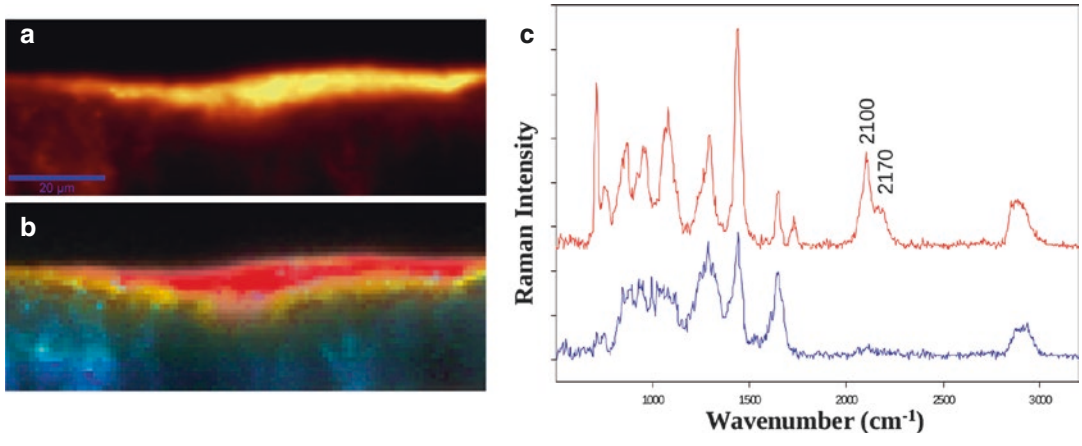

Fig. 15.13 XZ-profiles recorded on a full thickness human skin treated with deuterated invasomes. (**a**) Raman map generated by integrating C-H stretching intensities from 2800 to 3100 cm^{-1}. (**b**) False color image showing dissimilar spectral mixing. Red color represents highest C-D signal and while-blue represents signal from endogenous skin tissue. (**c**) The red spectra on the right are representative of the applied P-d_{31}OPC invasomes while blue spectra are representative of the skin. Peaks at 2100 and 2170 cm^{-1} represent C-D stretching vibrations

of the surfactant used and that an emulsified retinol can penetrate deeper in the skin, while micellar retinol is localized in the SC (Forster et al. 2011). Mélot et al. studied the effect of penetration enhancers to deliver retinol into human skin in vivo. The in vivo measurements were carried out using an inverted Raman microscope customized for fast in vivo spectral acquisition from volar forearm. Formulations containing penetration enhancers like oleic acid, polyethylene glycol showed to have improved penetration of retinol into SC after 6 h of application time (Mélot et al. 2009).

Caspers et al. used CRM to study the interactions between human skin and dimethyl sulfoxide (DMSO) in vivo (Caspers et al. 2002). DMSO shows strong C-S-C symmetric and asymmetric vibration modes at 671 and 702 cm^{-1}, while the position of the microscope in the skin was determined using the natural moisturizing factor to protein ratio (NMF, 885 & 1415 cm^{-1}). Authors reported that DMSO penetrated the SC within 20 min, however traces of DMSO could be found in the SC even after 72 h. Caspers et al. also reported the use of CRM for monitoring in vivo water profiles in the SC. Water content at various depths was determined by calculating the ratio of the water intensities (3350–3550 cm^{-1}) and protein intensities (CH_3 stretching mode 2910–2965 cm^{-1}). Chrit et al. also reported application of CRM for in vitro and in vivo measurement of water in human skin, and they were able to demonstrate the hydration efficiency of a cosmetic product containing hydrating polymers in microcapsules (Chrit et al. 2007).

CRM was used to follow the penetration of metronidazole dissolved in diethylene glycol monoethyl (Transcutol®, Gattefossé, France) in human skin (Tfayli et al. 2007). Metronidazole was tracked in the skin by monitoring (υ C-N) stretching vibrations at 1191 and 1369 cm^{-1}, while the skin proteins were tracked from the amide-I, amide-III, Phenylalanine-ring breathing mode and other weaker spectral features. Spectra were collected from full thickness skin 1 and 2 h after the application of metronidazole solution at different z-planes with 4 μm steps. Maximum penetration depth achieved for metronidazole was ~25 μm in the SC. Several changes were noted in the Raman shifts for C-H vibration bands associated with skin endogenous proteins and lipids. Zhang et al. took advantage of differences in the Raman spectra of 5-fluorouracil (5-FU) and the prodrug of 5-FU (1-ethoxycarbonyl-5-fluorouracil) to determine the spatial distribution and the transformation of prodrug to 5-FU in skin (Zhang et al. 2007).

15.5 Coherent Raman Microscopy

In spontaneous Raman microscopy, images are recorded using the mapping mode where Raman spectra from each point on the sample are collected. Due to the inherent weak nature of the Raman scattering, acquisition of such images can take several hours. This is a problem for biological samples as they can undergo dehydration or photo damage due to high exposure to the intense laser radiation. Today several variants of Raman microscopy are available, such as coherent anti-Stokes Raman scattering microscopy (CARS), stimulated Raman scattering microscopy (SRS), surface-enhanced Raman scattering (SERS), etc., which have an advantage of higher S/N ratio. In this part, we would like to introduce CARS and SRS in brief with some examples of their application in transdermal delivery research, but it is out of scope of this book to go in depth into the principles and instrumentation of these techniques; further references can be found elsewhere (Chabay et al. 1976; Cheng 2007; Eesley 1981; Nandakumar et al. 2009; Scholten and Scholten 1989; Scholten et al. 1989).

CARS and SRS are nonlinear enhancement techniques, which enhance the weak Raman signal and as a result reduce the imaging duration to a few minutes or even seconds (Hanson and Bardeen 2009). In both techniques the molecular vibrations are excited by using a Stokes and pump laser beams. CARS is a complex process in which three laser beams stokes (ω_s), pump (ω_p), and probe (ω_{pr}) interact with the sample to generate anti-stokes emission. When difference in the ω_s and ω_p frequencies approach the vibrational frequency of a molecular bond (ω_v), such that

$\omega_v = \omega_p - \omega_s$, the electrons in the electron cloud around the molecular bond are in the virtual excited vibrational state. Such vibrational excitations only take place in small focal volume where both stokes and pump beams are coherently in phase. To probe the virtual excitations, a third beam (ω_{pr}) is applied, which gets scattered off and generates anti-stokes radiation (ω_{as}) modulated at difference frequency such that $\omega_{as} = \omega_{pr} + (\omega_p - \omega_s)$ (Min et al. 2011). The emitted photon is blue shifted and as a result can be easily separated from the incident laser beams. Due to the nature of the excitation source of CARS microscope, it also generates 2-photon fluorescence and second harmonic generation (SHG) signal, and a multimodal detection system could be employed to detect these signals (Le et al. 2007; Potma et al. 2001; Wang et al. 2008).

The capability to identify endogenous and exogenous components by a multimodal-imaging mode is demonstrated in Fig. 15.14, which shows CARS, SHG, and 2-photon fluorescence signals collected from a human skin cross-section (Heuke et al. 2012). Figure 15.14a shows the anti-stokes Raman shifts recorded for C-H stretching mode at 2850 cm^{-1}, which are mainly generated by the intercellular lipids and adipocytes. Figure 15.14b shows the SHG signal, which is generated mainly from the collagen fibers of the dermis. Figure 15.14c shows 2-photon fluorescence detected at 435–485 nm, and Fig. 15.14d shows a false color image generated by overlapping all the signals, where CARS signal is represented as green, SHG as white, and two-photon fluorescence as red.

In vivo real-time video-rate epi-CARS (backscattered CARS) imaging was demonstrated by Evans et al. on anesthetized female mice (Evans et al. 2005). The excitation source was tuned in order to excite the CH_2 stretching vibrations and anti-Stokes photons were detected with the help of a sensitive PMT detector. The microscope had lateral resolution of 0.3 μm and axial resolution of 1.5 μm. Authors were able to image the mouse skin at various depth up to 100 μm and identified lipid rich structures such as sebaceous glands and adipocytes. Real time diffusion of the topically applied mineral oil was also observed in the mouse skin. The mineral oil penetrated the SC within 20 min, however it remained confined to

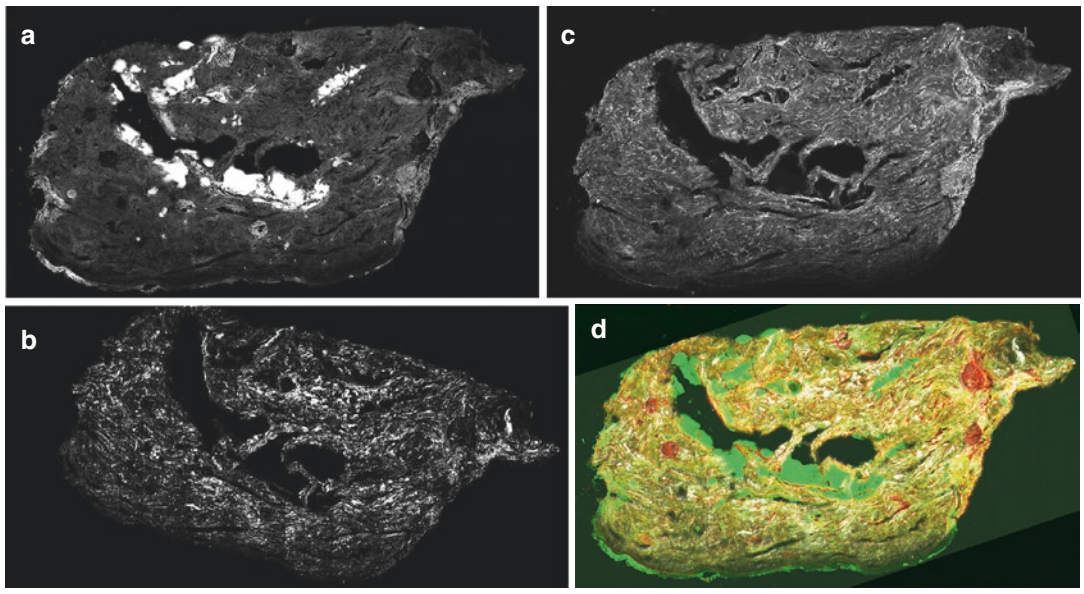

Fig. 15.14 Multimodal CARS image of an untreated skin cross-section to demonstrate the scope of multimodal microscopy. (**a**) CARS map for CH_2 symmetrical stretching vibrations, (**b**) SHG image, and (**c**) two-photon fluorescence image. (**d**) False color image showing overlap of CARS (*green*), SHG (*white*), and two-photon fluorescence (*red*) signals

the viable epidermis and was not able to penetrate the dermis. Zimmerley et al. used CARS microscopy to generate quantitative concentration maps of deuterated water and d-glycine in human hair (Zimmerley et al. 2009), while Breunig et al. demonstrated application of in vivo multimodal CARS microscopy in healthy and diseased human skin (Breunig et al. 2012). In healthy human skin, they were able to follow a topically applied emulsion cream, while in skin affected with psoriasis they were able to identify differences in the SC intercellular lipid domains compared to the healthy skin.

CARS microscopy is more sensitive than spontaneous Raman microscopy; however, it has some drawbacks such as the presence of non-resonant background and more importantly anti-Stokes shifts are slightly different from stokes Raman shifts, which makes spectral interpretation more complicated. In SRS, pump beam and stokes beam coincide the sample such that difference in the frequencies between Stokes and pump-beams matches a molecular vibration. This results in an increase in the rate of molecular vibrations. The energy required for this excitation is taken up from the pump laser field and as a result pump beam experiences loss in intensity (stimulated Raman loss). Stokes beam experiences a gain in intensity due to the emission of stokes photons as the molecular vibrations return to ground state (stimulated Raman gain). In SRS microscopy, either stimulated Raman loss or gain can be used as a contrast mechanism (Min et al. 2011; Nandakumar et al. 2009). Using SRS microscopy, Saar et al. were able to determine penetration profiles of ibuprofen and ketoprofen from solutions in propylene glycol applied topically onto mouse skin (Saar et al. 2011). Ketoprofen was tracked in the skin by following the aromatic C-H stretching vibrations at 1599 cm^{-1}, ibuprofen and propylene glycol were deuterated and were monitored at 2120 cm^{-1}, while skin lipid architecture was imaged from CH_2 stretching vibrations at 2845 cm^{-1}. Ketoprofen and propylene glycol penetrated the SC mainly via intercellular lipid pathways and through hair follicles. From time resolved images at various depths, the authors showed that propylene glycol penetrated deeper and faster than ketoprofen into the skin. In addition, penetration of propylene glycol via hair follicle was much faster and reached a steady state in less than 30 min compared to ~2 h via intercellular lipid penetration in the SC to reach similar levels. Penetration profiles of ibuprofen were similar to that of ketoprofen. Ibuprofen crystals on the surface of the SC during penetration also indicated faster penetration of the solvent propylene glycol compared to ibuprofen. Freudiger et al. reported application of SRS microscopy to construct three-dimensional diffusion profiles of DMSO and retinoic acid in mouse skin. From the diffusional profiles they were able to show that DMSO mainly penetrated the SC via the protein phase while retinoic acid penetrated mainly via the lipid rich intercellular spaces (Freudiger et al. 2008).

Coherent Raman microscopy is a label-free and more sensitive approach of tapping into the advantages of Raman effect compared to the spontaneous Raman microscopy. Due to the enhancement of the Raman effect, the image acquisition is much faster and hence more suitable for biological samples compared to spontaneous Raman microscopy. Also the nonlinear excitation approach in the generation of CARS and SRS signal is limited to a very small focal volume, which increases the resolution of these techniques without using the confocal detection setup. CARS and SRS microscopic techniques are relatively young compared to other techniques discussed here. Today these microscopes are mainly confined to the photonics labs; however, both the techniques hold a great promise for mainstream applications.

Conclusion

Microscopic techniques are very important in understanding the mechanisms involved in skin penetration as they enable spatial visualization of the drug in the skin. In this chapter, we report almost 50 years of development in the microscopic techniques and at least today, no technique holds superiority in all the aspects of imaging such as resolution, signal quality, specificity, speed, sample preparation, sample stability, etc. These are rather complementary

techniques, which are able to provide a host of information according to the requirements and objectives of the experiments. For skin penetration experiments, 2-PFM was first to set high standards owing to its ability to acquire high-resolution optical biopsies, in vitro as well as in vivo. Raman microscopic techniques provide a unique opportunity for label-free imaging. With development of modern Raman variants like CARS and SRS microscopy, the signal to noise ratio has been greatly improved and high speed, label free, 3D imaging is now possible however the complex nature of these microscopes and expensive optics have limited their widespread application.

Acknowledgment Authors would like to acknowledge Prof. Dr. Benjamin Dietzek and Prof. Dr. Jürgen Popp from Institut für Photonische Technologien, Jena, Germany, for their cooperation in acquiring multimodal CARS images on the human skin cross-sections.

References

Addicks WJ, Flynn GL, Weiner N (1987) Validation of a flow-through diffusion cell for use in transdermal research. Pharm Res 4(4):337–341

Agarwal R, Katare OP, Vyas SP (2000) The pilosebaceous unit: a pivotal route for topical drug delivery. Methods Find Exp Clin Pharmacol 22(2):129–133

Alvarez-Roman R, Naik A, Kalia YN, Guy RH, Fessi H (2004) Skin penetration and distribution of polymeric nanoparticles. J Control Release 99(1):53–62. doi:10.1016/j.jconrel.2004.06.015

Ashtikar M, Matthäus C, Krafft C, Popp J, Fahr A (2012) Non-invasive imaging of transdermal drug penetration profiles using Raman microscopy. 9th International conference and workshop on Biological Barriers – in vitro and in silico tools for drug delivery and nanosafety research, Saarland University, Saarbrücken, 29 Feb–9 Mar 2012

Benfeldt E (1999) In vivo microdialysis for the investigation of drug levels in the dermis and the effect of barrier perturbation on cutaneous drug penetration. Studies in hairless rats and human subjects. Acta Derm Venereol Suppl (Stockh) 206:1–59

Betz G, Imboden R, Imanidis G (2001) Interaction of liposome formulations with human skin in vitro. Int J Pharm 229(1–2):117–129

Bhatia KS, Singh J (1999) Effect of linolenic acid/ethanol or limonene/ethanol and iontophoresis on the in vitro percutaneous absorption of LHRH and ultrastructure of human epidermis. Int J Pharm 180(2):235–250

Bohm M, Luger TA (1998) The pilosebaceous unit is part of the skin immune system. Dermatology 196(1):75–79

Bouwstra JA, Honeywell-Nguyen PL (2002) Skin structure and mode of action of vesicles. Adv Drug Deliv Rev 54(Suppl 1):S41–S55

Breunig HG, Buckle R, Kellner-Hofer M, Weinigel M, Lademann J, Sterry W et al (2012) Combined in vivo multiphoton and CARS imaging of healthy and disease-affected human skin. Microsc Res Tech 75(4):492–498. doi:10.1002/jemt.21082

Carrer DC, Vermehren C, Bagatolli LA (2008) Pig skin structure and transdermal delivery of liposomes: a two photon microscopy study. J Control Release 132(1):12–20. doi:10.1016/j.jconrel.2008.08.006

Caspers PJ, Lucassen GW, Bruining HA, Puppels GJ (2000) Automated depth-scanning confocal Raman microspectrometer for rapid in vivo determination of water concentration profiles in human skin. J Raman Spectrosc 31(8–9):813–818. doi:10.1002/1097-4555(200008/09)31:8/9<813::AID-JRS573>3.0.CO;2-7

Caspers PJ, Williams AC, Carter EA, Edwards HG, Barry BW, Bruining HA et al (2002) Monitoring the penetration enhancer dimethyl sulfoxide in human stratum corneum in vivo by confocal Raman spectroscopy. Pharm Res 19(10):1577–1580

Chabay I, Klauminzer GK, Hudson BS (1976) Coherent anti-Stokes Raman spectroscopy (CARS): Improved experimental design and observation of new higher-order processes. Appl Phys Lett 28(1):27–29

Chen M, Liu X, Fahr A (2010) Skin delivery of ferulic acid from different vesicular systems. J Biomed Nanotechnol 6(5):577–585

Chen M, Liu X, Fahr A (2011) Skin penetration and deposition of carboxyfluorescein and temoporfin from different lipid vesicular systems: in vitro study with finite and infinite dosage application. Int J Pharm 408(1–2):223–234. doi:10.1016/j.ijpharm.2011.02.006

Cheng JX (2007) Coherent anti-Stokes Raman scattering microscopy. Appl Spectrosc 61(9):197–208

Chrit L, Bastien P, Biatry B, Simonnet JT, Potter A, Minondo AM et al (2007) In vitro and in vivo confocal Raman study of human skin hydration: assessment of a new moisturizing agent, pMPC. Biopolymers 85(4):359–369. doi:10.1002/bip.20644

Dragicevic-Curic N, Grafe S, Albrecht V, Fahr A (2008) Topical application of temoporfin-loaded invasomes for photodynamic therapy of subcutaneously implanted tumours in mice: a pilot study. J Photochem Photobiol B 91(1):41–50. doi:10.1016/j.jphotobiol.2008.01.009

Dragicevic-Curic N, Scheglmann D, Albrecht V, Fahr A (2009) Development of different temoporfin-loaded invasomes-novel nanocarriers of temoporfin: characterization, stability and in vitro skin penetration studies. Colloids Surf B Biointerfaces 70(2):198–206. doi:10.1016/j.colsurfb.2008.12.030

du Plessis J, Ramachandran C, Weiner N, Müller DG (1994) The influence of particle size of liposomes on

the deposition of drug into skin. Int J Pharm 103(3):277–282. doi:10.1016/0378-5173(94)90178-3
Du Q, Raksuntorn N, Younan NH, King RL (2008) End-member extraction for hyperspectral image analysis. Appl Opt 47(28):F77–F84
Dunn KW, Young PA (2006) Principles of multiphoton microscopy. Nephron Exp Nephrol 103(2):e33–e40
Eesley GL (1981) Coherent Raman spectroscopy, GL Eesley (ed). Pergamon Press, Oxford/New York
Evans CL, Potma EO, Puoris'haag M, Cote D, Lin CP, Xie XS (2005) Chemical imaging of tissue in vivo with video-rate coherent anti-Stokes Raman scattering microscopy. Proc Natl Acad Sci U S A 102(46):16807–16812. doi:10.1073/pnas.0508282102
Failloux N, Baron MH, Abdul-Malak N, Perrier E (2004) Contribution of encapsulation on the biodisponibility of retinol. Int J Cosmet Sci 26(2):71–77. doi:10.1111/j.0412-5463.2004.00206.x
Fang JY, Hsu LR, Huang YB, Tsai YH (1999) Evaluation of transdermal iontophoresis of enoxacin from polymer formulations: in vitro skin permeation and in vivo microdialysis using Wistar rat as an animal model. Int J Pharm 180(2):137–149
Forster M, Bolzinger MA, Ach D, Montagnac G, Briancon S (2011) Ingredients tracking of cosmetic formulations in the skin: a confocal Raman microscopy investigation. Pharm Res 28(4):858–872. doi:10.1007/s11095-010-0342-0
Freudiger CW, Min W, Saar BG, Lu S, Holtom GR, He C et al (2008) Label-free biomedical imaging with high sensitivity by stimulated Raman scattering microscopy. Science 322(5909):1857–1861. doi:10.1126/science.1165758
Grams YY, Alaruikka S, Lashley L, Caussin J, Whitehead L, Bouwstra JA (2003) Permeant lipophilicity and vehicle composition influence accumulation of dyes in hair follicles of human skin. Eur J Pharm Sci 18(5):329–336
Grams YY, Whitehead L, Cornwell P, Bouwstra JA (2004) Time and depth resolved visualisation of the diffusion of a lipophilic dye into the hair follicle of fresh unfixed human scalp skin. J Control Release 98(3):367–378. doi:10.1016/j.jconrel.2004.05.010
Hanson KM, Bardeen CJ (2009) Application of nonlinear optical microscopy for imaging skin. Photochem Photobiol85(1):33–44.doi:10.1111/j.1751-1097.2008.00508.x
Hashimoto K, Kagetsu N, Taniguchi Y, Weintraub R, Chapman-Winokur RL, Kasiborski A (1991) Immunohistochemistry and electron microscopy in Langerhans cell histiocytosis confined to the skin. J Am Acad Dermatol 25(6 Pt 1):1044–1053
Heuke S, Ashtikar M, Matthäus C, Fahr A, Dietzek B, Popp J (2012) Coherent anti-stokes Raman scattering microscopy of human skin (Unpublished data)
Hofland HE, van der Geest R, Bodde HE, Junginger HE, Bouwstra JA (1994) Estradiol permeation from non-ionic surfactant vesicles through human stratum corneum in vitro. Pharm Res 11(5):659–664
Hofland HE, Bouwstra JA, Bodde HE, Spies F, Junginger HE (1995) Interactions between liposomes and human stratum corneum in vitro: freeze fracture electron microscopical visualization and small angle X-ray scattering studies. Br J Dermatol 132(6):853–866
Hollricher O (2011) Raman instrumentation for confocal Raman microscopy. In: Dieing T, Hollricher O, Toporski J (eds) Confocal Raman microscopy, Springer Series in Optical Sciences. 158. Springer, Berlin/Heidelberg, pp 43–60
Hollricher O, Ibach W (2011) High-resolution optical and confocal microscopy. In: Dieing T, Hollricher O, Toporski J (eds) Confocal Raman microscopy, Springer Series in Optical Sciences. 158. Springer, Berlin/Heidelberg, pp 1–20
Jimbo Y, Ishihara M, Osamura H, Takano M, Ohara M (1983) Influence of vehicles on penetration through human epidermis of benzyl alcohol, isoeugenol and methyl isoeugenol. J Dermatol 10(3):241–250
Kanerva L (1990) Electron microscopy of the effects of dithranol on healthy and on psoriatic skin. Am J Dermatopathol 12(1):51–62
Kirjavainen M, Urtti A, Jaaskelainen I, Suhonen TM, Paronen P, Valjakka-Koskela R et al (1996) Interaction of liposomes with human skin in vitro--the influence of lipid composition and structure. Biochim Biophys Acta 1304(3):179–189
Kirjavainen M, Urtti A, Monkkonen J, Hirvonen J (2000) Influence of lipids on the mannitol flux during transdermal iontophoresis in vitro. Eur J Pharm Sci 10(2):97–102
Kobayashi D, Matsuzawa T, Sugibayashi K, Morimoto Y, Kimura M (1994) Analysis of the combined effect of 1-menthol and ethanol as skin permeation enhancers based on a two-layer skin model. Pharm Res 11(1):96–103
Konig K, Ehlers A, Stracke F, Riemann I (2006) In vivo drug screening in human skin using femtosecond laser multiphoton tomography. Skin Pharmacol Physiol 19(2):78–88. doi:10.1159/000091974
Kriwet K, Müller-Goymann CC (1995) Diclofenac release from phospholipid drug systems and permeation through excised human stratum corneum. Int J Pharm 125(2):231–242. doi:10.1016/0378-5173(95)00130-B
Le TT, Langohr IM, Locker MJ, Sturek M, Cheng JX (2007) Label-free molecular imaging of atherosclerotic lesions using multimodal nonlinear optical microscopy. J Biomed Opt 12(5):054007. doi:10.1117/1.2795437
Lieb LM, Ramachandran C, Egbaria K, Weiner N (1992) Topical delivery enhancement with multilamellar liposomes into pilosebaceous units: I. In vitro evaluation using fluorescent techniques with the hamster ear model. J Invest Dermatol 99(1):108–113
Loftsson T, Somogyi G, Bodor N (1989) Effect of choline esters and oleic acid on the penetration of acyclovir, estradiol, hydrocortisone, nitroglycerin, retinoic acid and trifluorothymidine across hairless mouse skin in vitro. Acta Pharm Nord 1(5):279–286

Mélot M, Pudney PDA, Williamson A-M, Caspers PJ, Van Der Pol A, Puppels GJ (2009) Studying the effectiveness of penetration enhancers to deliver retinol through the stratum cornum by in vivo confocal Raman spectroscopy. J Control Release 138(1):32–39. doi:10.1016/j.jconrel.2009.04.023

Min W, Freudiger CW, Lu S, Xie XS (2011) Coherent nonlinear optical imaging: beyond fluorescence microscopy. Annu Rev Phys Chem 62:507–530. doi:10.1146/annurev.physchem.012809.103512

Murakami T, Yoshioka M, Yumoto R, Higashi Y, Shigeki S, Ikuta Y et al (1998) Topical delivery of keloid therapeutic drug, tranilast, by combined use of oleic acid and propylene glycol as a penetration enhancer: evaluation by skin microdialysis in rats. J Pharm Pharmacol 50(1):49–54

Nandakumar P, Kovalev A, Volkmer A (2009) Vibrational imaging based on stimulated Raman scattering microscopy. New J Phys 11(3):033026

Niemiec SM, Ramachandran C, Weiner N (1995) Influence of nonionic liposomal composition on topical delivery of peptide drugs into pilosebaceous units: an in vivo study using the hamster ear model. Pharm Res 12(8):1184–1188

Ntimenou V, Fahr A, Antimisiaris SG (2012) Elastic vesicles for transdermal drug delivery of hydrophilic drugs: a comparison of important physicochemical characteristics of different vesicle types. J Biomed Nanotechnol 8(4):613–623

Nwaneshiudu A, Kuschal C, Sakamoto FH, Anderson RR, Schwarzenberger K, Young RC (2012) Introduction to confocal microscopy. J Invest Dermatol 132(12), e3. doi:10.1038/jid.2012.429

Patzelt A, Richter H, Knorr F, Schäfer U, Lehr C-M, Dähne L et al (2011) Selective follicular targeting by modification of the particle sizes. J Control Release 150(1):45–48. doi:http://dx.doi.org/10.1016/j.jconrel.2010.11.015

Potma EO, de Boeij WP, van Haastert PJM, Wiersma DA (2001) Real-time visualization of intracellular hydrodynamics in single living cells. Proc Natl Acad Sci 98(4):1577–1582. doi:10.1073/pnas.98.4.1577

Raman C, Krishnan K (1928) A new type of secondary radiation. Nature 121(3048):501–502. doi:10.1038/121501c0

Saar BG, Contreras-Rojas LR, Xie XS, Guy RH (2011) Imaging drug delivery to skin with stimulated Raman scattering microscopy. Mol Pharm 8(3):969–975. doi:10.1021/mp200122w

Schatzlein A, Cevc G (1998) Non-uniform cellular packing of the stratum corneum and permeability barrier function of intact skin: a high-resolution confocal laser scanning microscopy study using highly deformable vesicles (Transfersomes). Br J Dermatol 138(4):583–592

Schenke-Layland K, Riemann I, Damour O, Stock UA, Konig K (2006) Two-photon microscopes and in vivo multiphoton tomographs--powerful diagnostic tools for tissue engineering and drug delivery. Adv Drug Deliv Rev 58(7):878–896. doi:10.1016/j.addr.2006.07.004

Schnetz E, Fartasch M (2001) Microdialysis for the evaluation of penetration through the human skin barrier - a promising tool for future research? Eur J Pharm Sci 12(3):165–174

Scholten T, Scholten TAHM (1989) Coherent Anti-stokes Raman Scattering (CARS): technique and application to biophysical studies; the potentials of CARS microscopy

Scholten TA, Lucassen GW, De Mul FF, Greve J (1989) Nonresonant background suppression in CARS spectra of dispersive media using phase mismatching. Appl Opt 28(7):1387–1400. doi:10.1364/ao.28.001387

Schreiner V, Gooris GS, Pfeiffer S, Lanzendorfer G, Wenck H, Diembeck W et al (2000) Barrier characteristics of different human skin types investigated with X-ray diffraction, lipid analysis, and electron microscopy imaging. J Invest Dermatol 114(4):654–660. doi:10.1046/j.1523-1747.2000.00941.x

Semwogerere D, Weeks ER (2008) Confocal microscopy. In: Encyclopedia of biomaterials and biomedical engineering. Informa Healthcare, New York, pp 705–714

Simonetti O, Hoogstraate AJ, Bialik W, Kempenaar JA, Schrijvers AH, Bodde HE et al (1995) Visualization of diffusion pathways across the stratum corneum of native and in-vitro-reconstructed epidermis by confocal laser scanning microscopy. Arch Dermatol Res 287(5):465–473

Tenjarla SN, Kasina R, Puranajoti P, Omar MS, Harris WT (1999) Synthesis and evaluation of N-acetylprolinate esters – novel skin penetration enhancers. Int J Pharm 192(2):147–158

Tfayli A, Piot O, Pitre F, Manfait M (2007) Follow-up of drug permeation through excised human skin with confocal Raman microspectroscopy. Eur Biophys J 36(8):1049–1058. doi:10.1007/s00249-007-0191-x

Touitou E, Godin B, Dayan N, Weiss C, Piliponsky A, Levi-Schaffer F (2001) Intracellular delivery mediated by an ethosomal carrier. Biomaterials 22(22):3053–3059

Turner NG, Guy RH (1998) Visualization and quantitation of iontophoretic pathways using confocal microscopy. J Investig Dermatol Symp Proc 3(2):136–142

van den Bergh BA, Vroom J, Gerritsen H, Junginger HE, Bouwstra JA (1999) Interactions of elastic and rigid vesicles with human skin in vitro: electron microscopy and two-photon excitation microscopy. Biochim Biophys Acta 1461(1):155–173

van Kuijk-Meuwissen ME, Junginger HE, Bouwstra JA (1998a) Interactions between liposomes and human skin in vitro, a confocal laser scanning microscopy study. Biochim Biophys Acta 1371(1):31–39

van Kuijk-Meuwissen ME, Mougin L, Junginger HE, Bouwstra JA (1998b) Application of vesicles to rat skin in vivo: a confocal laser scanning microscopy study. J Control Release 56(1–3):189–196

Vardaxis NJ, Brans TA, Boon ME, Kreis RW, Marres LM (1997) Confocal laser scanning microscopy of porcine skin: implications for human wound healing studies. J Anat 190(Pt 4):601–611

Veiro JA, Cummins PG (1994) Imaging of skin epidermis from various origins using confocal laser scanning microscopy. Dermatology 189(1):16–22

Verma D (2002) Thesis title: invasomes – novel vesicular carriers for enhanced topical delivery: characterization and skin penetration properties. Philipps-Universität Marburg, Marburg

Verma DD, Fahr A (2004) Synergistic penetration enhancement effect of ethanol and phospholipids on the topical delivery of cyclosporin A. J Control Release 97(1):55–66. doi:10.1016/j.jconrel.2004.02.028

Verma DD, Verma S, Blume G, Fahr A (2003a) Particle size of liposomes influences dermal delivery of substances into skin. Int J Pharm 258(1–2):141–151

Verma DD, Verma S, Blume G, Fahr A (2003b) Liposomes increase skin penetration of entrapped and non-entrapped hydrophilic substances into human skin: a skin penetration and confocal laser scanning microscopy study. Eur J Pharm Biopharm 55(3):271–277

Verma DD, Verma S, McElwee KJ, Freyschmidt-Paul P, Hoffmann R, Fahr A (2004) Treatment of alopecia areata in the DEBR model using cyclosporin A lipid vesicles. Euro J Dermatol 14(5):1–7

Wang HW, Le TT, Cheng JX (2008) Label-free imaging of arterial cells and extracellular matrix using a multimodal CARS microscope. Opt Commun 281(7):1813–1822. doi:10.1016/j.optcom.2007.07.067

Wascotte V, Caspers P, de Sterke J, Jadoul M, Guy RH, Preat V (2007) Assessment of the "skin reservoir" of urea by confocal Raman microspectroscopy and reverse iontophoresis in vivo. Pharm Res 24(10):1897–1901. doi:10.1007/s11095-007-9314-4

Winter ME (1999) N-FINDR: an algorithm for fast autonomous spectral end-member determination in hyperspectral data. Proc SPIE. 266–75. doi:10.1117/12.366289.

Xiao C, Moore DJ, Rerek ME, Flach CR, Mendelsohn R (2005) Feasibility of tracking phospholipid permeation into skin using infrared and Raman microscopic imaging. J Invest Dermatol 124(3):622–632. doi:10.1111/j.0022-202X.2004.23608.x

Yarosh D, Bucana C, Cox P, Alas L, Kibitel J, Kripke M (1994) Localization of liposomes containing a DNA repair enzyme in murine skin. J Invest Dermatol 103(4):461–468

Yu B, Kim KH, So PT, Blankschtein D, Langer R (2003) Visualization of oleic acid-induced transdermal diffusion pathways using two-photon fluorescence microscopy. J Invest Dermatol 120(3):448–455. doi:10.1046/j.1523-1747.2003.12061.x

Zellmer S, Reissig D, Lasch J (1998) Reconstructed human skin as model for liposome-skin interaction. J Control Release 55(2–3):271–279

Zhang G, Moore DJ, Sloan KB, Flach CR, Mendelsohn R (2007) Imaging the prodrug-to-drug transformation of a 5-fluorouracil derivative in skin by confocal Raman microscopy. J Invest Dermatol 127(5):1205–1209. doi:10.1038/sj.jid.5700690

Zimmerley M, Lin C-Y, Oertel DC, Marsh JM, Ward JL, Potma EO (2009) Quantitative detection of chemical compounds in human hair with coherent anti-Stokes Raman scattering microscopy. J Biomed Opt 14(4):044019. doi:10.1117/1.3184444